Journal of the American College of Cardiology
© 2005 by the American College of Cardiology Foundation
Published by Elsevier Inc.

Vol. 45, No. 2, 2005
ISSN 0735-1097/05/$30.00
doi:10.1016/j.jacc.2004.09.069

Cellular and Ionic Mechanism for Drug-Induced Long QT Syndrome and Effectiveness of Verapamil

Takeshi Aiba, MD, PHD,* Wataru Shimizu, MD, PHD,† Masashi Inagaki, MD,* Takashi Noda, MD, PHD,* Shunichiro Miyoshi, MD, PHD,‡ Wei-Guang Ding, MD, PHD,§ Dimitar P. Zankov, MD,§‖ Futoshi Toyoda, PHD,§ Hiroshi Matsuura, MD, PHD,§ Minoru Horie, MD, PHD,‖ Kenji Sunagawa, MD, PHD*

Osaka, Tokyo, and Shiga, Japan

OBJECTIVES We examined the cellular and ionic mechanism for QT prolongation and subsequent Torsade de Pointes (TdP) and the effect of verapamil under conditions mimicking *KCNQ1* (I_{Ks} gene) defect linked to acquired long QT syndrome (LQTS).

BACKGROUND Agents with an I_{Kr}-blocking effect often induce marked QT prolongation in patients with acquired LQTS. Previous reports demonstrated a relationship between subclinical mutations in cardiac K^+ channel genes and a risk of drug-induced TdP.

METHODS Transmembrane action potentials from epicardial (EPI), midmyocardial (M), and endocardial (ENDO) cells were simultaneously recorded, together with a transmural electrocardiogram, at a basic cycle length of 2,000 ms in arterially perfused feline left ventricular preparations.

RESULTS The I_{Kr} block (E-4031: 1 μmol/l) under control conditions (n = 5) prolonged the QT interval but neither increased transmural dispersion of repolarization (TDR) nor induced arrhythmias. However, the I_{Kr} blocker under conditions with I_{Ks} suppression by chromanol 293B 10 μmol/l mimicking the *KCNQ1* defect (n = 10) preferentially prolonged action potential duration (APD) in EPI rather than M or ENDO, thereby dramatically increasing the QT interval and TDR. Spontaneous or epinephrine-induced early afterdepolarizations (EADs) were observed in EPI, and subsequent TdP occurred only under both I_{Ks} and I_{Kr} suppression. Verapamil (0.1 to 5.0 μmol/l) dose-dependently abbreviated APD in EPI more than in M and ENDO, thereby significantly decreasing the QT interval, TDR, and suppressing EADs and TdP.

CONCLUSIONS Subclinical I_{Ks} dysfunction could be a risk of drug-induced TdP. Verapamil is effective in decreasing the QT interval and TDR and in suppressing EADs, thus preventing TdP in the model of acquired LQTS. (J Am Coll Cardiol 2005;45:300–7) © 2005 by the American College of Cardiology Foundation

The long QT syndrome (LQTS) is characterized by a prolongation of ventricular repolarization and recurrent episodes of atypical polymorphic ventricular tachycardia known as Torsade de Pointes (TdP) leading to sudden cardiac death (1–3). The molecular basis of congenital LQTS is attributed to defects in several ion channel genes encoding delayed rectifier K^+ or Na^+ currents. On the other hand, agents that block rapidly activating delayed rectifier potassium current (I_{Kr}) often induce marked QT prolongation with an inverted T wave in patients with acquired LQTS. Recent studies indicate that some cases of drug-induced LQTS can be associated with silent mutations and common polymorphism in genes responsible for the congenital LQTS (4), such as *KCNQ1* encoding slowly activating delayed rectifier potassium currents (I_{Ks}) (5–7). However, it remains unclear why subclinical I_{Ks} dysfunction is a risk of drug-induced LQTS.

Both early afterdepolarization (EAD)-induced triggered activity and increased dispersion of repolarization have been suggested as important in the genesis of ventricular arrhythmias in congenital and acquired LQTS. Moreover, verapamil, an L-type Ca^{2+} channel blocker, suppressed EADs and TdP in patients with LQTS (8,9). In the present study, we hypothesized that: 1) addition of I_{Kr} block to I_{Ks} dysfunction markedly prolongs action potential duration (APD) and induces TdP by producing EADs and/or increases transmural dispersion of repolarization (TDR); and 2) verapamil suppresses TdP by preventing EADs and decreasing TDR. In arterially perfused feline left ventricular wedge preparations, we demonstrated that subclinical I_{Ks} dysfunction, mimicking *KCNQ1* defect, could be a risk of drug-induced TdP, and verapamil successfully suppressed TdP in the model of acquired LQTS.

METHODS

Arterially perfused wedge preparations and electrophysiologic recordings. All animal care procedures were in accordance with the position of the American Heart Association research animal use (November 11, 1984). The

From the *Department of Cardiovascular Dynamics, Research Institute, and †Division of Cardiology, Department of Internal Medicine, National Cardiovascular Center, Suita, Osaka, Japan; the ‡Department of Physiology, Keio University School of Medicine, Tokyo, Japan; §Department of Physiology and ‖Department of Cardiovascular and Respiratory Medicine, Shiga University of Medical Science, Otsu, Shiga, Japan. This study was supported by the Program for Promotion of Fundamental Studies in Health Science of the Organization for Pharmaceutical Safety and Research (of Japan) (to Dr. Sunagawa), a grant from the Japan Cardiovascular Research Foundation (to Dr. Aiba), Fukuda Foundation for Medical Technology (to Dr. Inagaki), Vehicle Racing Commemorative Foundation (to Dr. Shimizu), Health Sciences Research Grants from the Ministry of Health, Labour and Welfare (to Dr. Shimizu), and the Research grant for Cardiovascular Disease (15C-6) from the Ministry of Health, Labour and Welfare (to Dr. Shimizu).

Manuscript received August 24, 2004; revised manuscript received September 21, 2004, accepted September 28, 2004.

Abbreviations and Acronyms

APD_{90} = action potential duration measured at 90% repolarization
BCL = basic cycle length
EAD = early afterdepolarization
I_K = delayed rectifier potassium current
I_{Kr} = rapidly activating delayed rectifier potassium current
I_{Ks} = slowly activating delayed rectifier potassium current
LQTS = long QT syndrome
TdP = Torsade de Pointes
TDR = transmural dispersion of repolarization

methods used for isolation, perfusion, and recording of transmembrane activity from the arterially perfused feline left ventricle have been detailed in a previous study (10) and are similar to methods reported using canine or rabbit wedge preparations (11–15). Briefly, a transmural wedge was dissected from the anterior wall of the left ventricle, cannulated via the left descending coronary artery (or the first branch of the left circumflex), and placed in a small tissue bath arterially perfused with Tyrode's solution. The temperature was maintained at 37 ± 1°C and perfusion pressure maintained between 40 and 60 mm Hg. Ventricular wedges were stimulated with bipolar electrodes applied to the endocardial surface. We recorded a transmural electrocardiogram (ECG) (epicardial, positive pole) using Ag-AgCl electrodes, and transmembrane action potentials (APs) simultaneously from the epicardium, midmyocardium (M), and endomyocardium using three separate intracellular floating microelectrodes. The epicardial and endocardial APs were recorded from the epicardial and endocardial surfaces, respectively, at positions approximating the transmural axis of the ECG. The M-cell's AP was recorded from the transmural surface, mainly at the subendocardium, along the same axis.

An I_{Kr} blocker, E-4031 1 μmol/l, was used in control condition (n = 5) or under condition with I_{Ks} suppression by chromanol 293B 10 μmol/l, mimicking *KCNQ1* defect (n = 10). The effects of an L-type Ca^{2+} channel blocker, verapamil, were evaluated at 0.1, 1, 2.5, and 5 μmol/l under the I_{Ks} and I_{Kr} suppression (acquired LQTS condition). Epinephrine 0.5 μmol/l was used to mimic increased sympathetic activity in the absence and presence of verapamil under the acquired LQTS condition. The spontaneous or epinephrine-induced EADs and subsequent TdP were evaluated under each set of conditions.

Data using E-4031, 293B, 293B + E-4031, and additional verapamil on top of 293B + E-4031 were collected for a period of 30 min starting 30 min after applying the above compounds to the perfusion. The APD was measured at 90% repolarization (APD_{90}). The TDR was defined as the difference between the longest and shortest repolarization times (activation time + APD_{90}) of the APs recorded across the wall. The QT interval was defined as the time interval between the QRS onset and the point at which the line of maximal downslope of the positive T wave and the line of the maximal upslope of the negative T wave crossed the baseline.

Whole-cell patch-clamp experiments. Epicardial, M, and endocardial cells isolated from the feline left ventricle were voltage-clamped using whole-cell configuration of the patch-clamp technique (16). Patch electrodes were pulled from borosilicate glass capillaries, heat-polished, and had a tip resistance of 2.0 to 3.0 MΩ when filled with standard pipette solution containing (mmol/l): 70 potassium aspartate, 50 KCl, 10 KH_2PO_4, 1 $MgSO_4$, 3 Na_2-ATP, 0.1 Li_2-GTP, 5 EGTA, and 5 HEPES (pH adjusted to 7.2 with KOH). Membrane currents were recorded from the epicardial, M, and endocardial cells superfused at 34 to 36°C with normal Tyrode's solution containing (mmol/l): 140 NaCl, 5.4 KCl, 1.8 $CaCl_2$, 0.5 $MgCl_2$, 0.33 NaH_2PO_4, 5.5 glucose, and 5.0 HEPES (pH adjusted to 7.4 with NaOH). In all current measurements, nisoldipine (0.4 μmol/l) was added to normal Tyrode's solution to abolish $I_{Ca,L}$. The cell membrane capacitance (C_m) was calculated for each cell by fitting the single exponential function to the decay of the capacitive transient elicited by a 5-mV step hyperpolarization applied from a holding potential of −50 mV (17).

Simulation study. Isolated epicardial, M, and endocardial cells were simulated using a Luo-Rudy dynamic cell model modified by varying the maximum conductance (density) of I_{Kr} and I_{Ks} (G_{Kr} and G_{Ks}) as described previously (18), in which the G_{Ks}/G_{Kr} in the epicardial, M, and endocardial cells were 23, 17, and 19, respectively. The transient outward potassium current (I_{to}) was incorporated into the model using the formulation of Dumaine et al. (19), in which the maximum conductance of I_{to} (G_{to}) was set to 0.5, 0.25, and 0.05 mS/μF in the epicardial, M, and endocardial cells, respectively.

Statistics. Statistical analysis of the data was performed with a Student *t* test for paired data or analysis of variance coupled with Bonferroni's test, as appropriate. Data are expressed as mean values ± SD except for those shown in the figures, which are expressed as mean ± SEM. Significance was defined as a value of $p < 0.05$.

RESULTS

The QT interval, APD, and TDR under an acquired LQTS condition with or without epinephrine. Figure 1 shows transmembrane activity recorded simultaneously from the epicardium, M, and endocardium together with a transmural ECG at a basic cycle length (BCL) of 2,000 ms. E-4031 (1 μmol/l) alone significantly, but homogenously, prolonged APD of the three regions, causing no major change in TDR (Fig. 1B). Chromanol 293B (10 μmol/l) alone did not significantly increase the QT interval, APD of the three regions, and TDR (Fig. 1C). The additional E-4031 to 293B, mimicking acquired LQTS, preferentially prolonged epicardial APD, thus dramatically increased QT

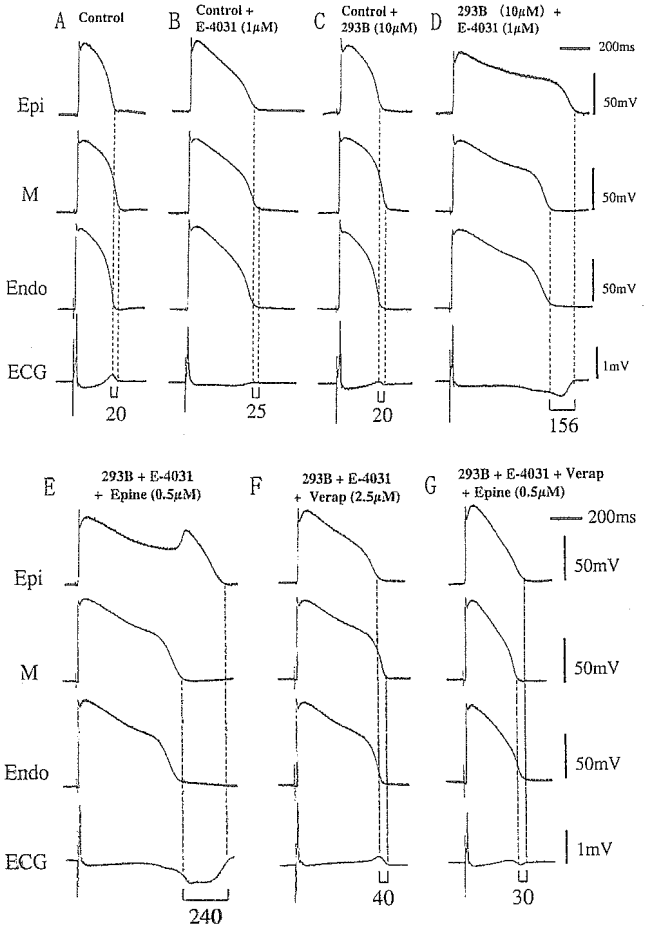

Figure 1. Transmembrane action potentials simultaneously recorded from the epicardial (Epi), midmyocardial (M), and endocardial (Endo) regions and a transmural electrocardiogram (ECG) at basic cycle length of 2,000 ms under each study condition. **(A)** Control. **(B)** E-4031 (1 μmol/l). **(C)** Chromanol 293B (10 μmol/l). **(D)** 293B + E-4031 (acquired long QT syndrome [LQTS] condition). **(E)** Epinephrine infusion (Epine: 0.5 μmol/l) under acquired LQTS condition. **(F)** Addition of verapamil (Verap) 2.5 μmol/l under acquired LQTS condition. **(G)** Further addition of Epine in the continued presence of Verap under acquired LQTS condition. Numbers at bottom of each ECG denote transmural dispersion of repolarization (ms).

interval and TDR (Fig. 1D). Epinephrine infusion (0.5 μmol/l) further prolonged epicardial APD associated with induction of EADs, but did not prolong M or endocardial

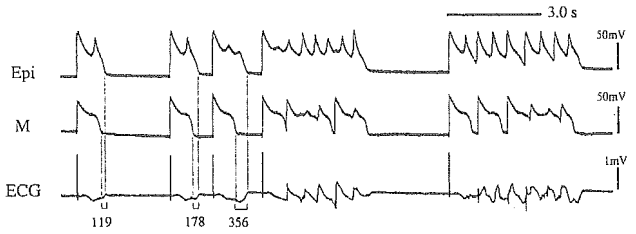

Figure 2. Spontaneous early afterdepolarization and subsequent Torsade de Pointes under the acquired long QT syndrome condition (293B 10 μmol/l + E-4031 1 μmol/l). Basic cycle length = 3,000 ms. Recordings and abbreviations as in Figure 1.

APD, resulting in further QT prolongation and increasing TDR (Fig. 1E).

The composite data of the QT interval, APD_{90} of the epicardium, M, and endocardium, and TDR at a BCL of 2,000 ms are shown in Table 1. E-4031 under control significantly, but homogeneously, prolonged APD_{90}, resulting in neither change of TDR nor induction of arrhythmia. Chromanol 293B under control did not significantly increase APD_{90} of the three regions, resulting in no major change in QT interval and TDR. Whereas additional E-4031 to 293B markedly prolonged QT interval as evidenced by preferential prolongation of the epicardial APD_{90} compared with M and endocardial APD_{90}, thus dramatically increased TDR. Epinephrine further prolonged the epicardial APD_{90}, but shortened the M region APD_{90}, resulting in further prolongation of the QT interval and increasing TDR.

Neither E-4031 alone nor 293B alone produced any EADs or TdP. However, additional E-4031 to 293B (acquired LQTS condition) induced spontaneous EADs from the epicardium in 5 of 10 preparations, including two preparations with spontaneous TdP (Fig. 2), but not from the M or endocardium. Further epinephrine infusion (n = 8) induced EADs from the epicardium in all preparations, including four preparations with subsequent TdP, but EADs from the M region were seen in only one preparation.

Effect of verapamil on the QT interval, APD, TDR, and induction of arrhythmias under an acquired LQTS condition. Under the acquired LQTS condition, verapamil dose-dependently (0.1 to 5 μmol/l) abbreviated APD of

Table 1. Effect of I_{Kr} Block With or Without Pretreated I_{Ks} Block on the QT Interval, APD_{90}, and Transmural Dispersion of Repolarization

		APD_{90}			
	QT	Epi	M	Endo	TDR
Control (n = 5)	283 ± 15	227 ± 16	259 ± 8	246 ± 13	31 ± 10
E-4031 (1 μM) (n = 5)	446 ± 42*	373 ± 30*	408 ± 28*	374 ± 25*	34 ± 4
Control (n = 10)	279 ± 12	230 ± 16	253 ± 14	237 ± 19	24 ± 5
293B (10 μM) (n = 10)	298 ± 34	252 ± 26	275 ± 33	253 ± 16	24 ± 9
293B (10 μM) + E-4031 (1 μM) (n = 10)	793 ± 183*	723 ± 164*	596 ± 131*	545 ± 78*	175 ± 68*
293B + E-4031 + Epine (0.5 μM) (n = 8)	866 ± 251	801 ± 217	506 ± 123	525 ± 118	191 ± 75
293B + E-4031 + Verap (2.5 μM) (n = 7)	557 ± 178‡	503 ± 171‡	483 ± 135†	516 ± 154	35 ± 37‡
293B + E-4031 + Verap + Epine (n = 6)	445 ± 113‡	403 ± 117‡	399 ± 93‡	411 ± 98†	30 ± 12‡

*$p < 0.001$ vs. control, †$p < 0.05$ vs. 293B + E-4031; ‡$p < 0.01$ vs. 293B + E-4031 by analysis of variance with Bonferroni's test.

APD_{90} = action potential duration at 90% repolarization; Endo = endocardium; Epi = epicardium; Epine = epinephrine; I_{Ks} = slowly activating delayed rectifier potassium current; I_{Kr} = rapidly activating delayed rectifier potassium current; M = mid-myocardium; QT = QT interval; TDR = transmural dispersion of repolarization; Verap = verapamil.

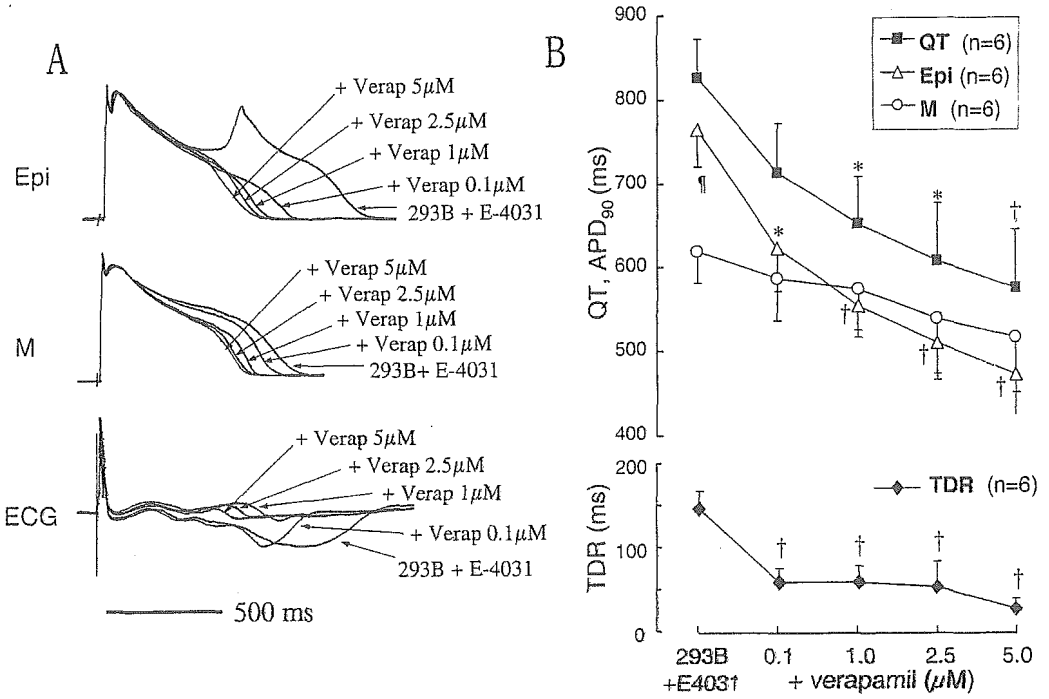

Figure 3. Dose-dependent effect of Verap (0.1 to 5 μmol/l) on transmembrane and ECG activity under acquired LQTS condition (293B 10 μmol/l + E-4031 1 μmol/l). **(A)** Superimposed action potentials recorded simultaneously from the epicardial and M regions together with a transmural ECG. **(B)** Composite data of the effect of Verap on QT interval **(solid squares)**, action potential duration measured at 90% repolarization (APD_{90}) of Epi **(open triangles)** and M **(open circles)** regions and transmural dispersion of repolarization (TDR) **(solid diamonds)**. Basic cycle length = 2,000 ms. *$p < 0.05$ vs. 293B + E-4031; †$p < 0.01$ vs. 293B + E-4031; ¶$p < 0.05$ vs. M region by analysis of variance with Bonferroni's test. Abbreviations as in Figure 1.

the epicardial and M regions as well as the QT interval (Fig. 3A). Figure 3B shows composite data of the dose-dependent effect of verapamil on the QT interval, APD_{90} of the epicardial and M regions, and TDR under the acquired LQTS condition (n = 6). A 5-μmol/l dose of verapamil under the acquired LQTS condition preferentially abbreviated the epicardial APD_{90} (761 ± 99 ms to 469 ± 95 ms; $p < 0.001$) compared with the M region APD_{90} (615 ± 83 ms to 512 ± 146 ms; p = NS), resulting in a significant decrease in TDR (146 ± 46 ms to 26 ± 28 ms; $p < 0.01$). The change in QT interval paralleled the decrease in the epicardial APD_{90}.

As shown in Figure 1F, 2.5-μmol/l verapamil preferentially abbreviated the epicardial APD_{90} rather than the M or endocardium, thus significantly abbreviated QT interval and TDR. Moreover, verapamil completely prevented the influence of epinephrine in inducing EADs and TdP as well as increasing the epicardial APD_{90}, QT interval, and TDR (Fig. 1G). The composite data of the effect of verapamil on the QT interval, APD, and TDR with or without epinephrine are shown in Table 1. Thus, verapamil totally suppressed EADs and TdP under the acquired LQTS condition with or without epinephrine.

Measurement of I_{Kr} and I_{Ks} in epicardial, M, and endocardial cells. Figure 4A represents the dose-dependent inhibition of I_{Ks} by 293B in an epicardial cell. Figure 4B illustrates the concentration-response relationships for the inhibition of I_{Ks} tail current. The data points were reasonably well described by a Hill equation with the following parameters: IC_{50} = 6.39 ± 1.17 μmol/l, n_H = 1.23 ± 0.05 (epicardial cells: n = 5); IC_{50} = 5.71 ± 1.32 μmol/l, n_H = 1.25 ± 0.12 (M cells: n = 5); IC_{50} = 5.73 ± 0.94 μmol/l, n_H = 1.07 ± 0.19 (endocardial cells: n = 5). There are no significant differences in IC_{50} and n_H values among the epicardial, M, and endocardial cells (analysis of variance with Bonferroni's test), thus indicating that I_{Ks} in these three cell types represents a similar sensitivity to inhibition by chromanol 293B.

Figure 5 represents the sensitivity of I_K to blockers of I_{Kr} and I_{Ks} (E-4031 and 293B, respectively). After the I_K reached a practically steady level (control, trace 1), application of E-4031 (3 μmol/l) markedly reduced the amplitude of I_K tail current (trace 2), and further addition of 293B (30 μmol/l) almost completely abolished the I_K tail current (trace 3). Table 2 summarizes densities of I_{Kr} and I_{Ks} in the epicardial, M, and endocardial cells, determined as E-4031- and 293B-sensitive tail currents normalized with reference to C_m. In each cell type, the density of I_{Ks} was significantly smaller than that of I_{Kr}. The density of I_{Kr} was almost equivalent among the three cell types, whereas I_{Ks} density was significantly smaller in M cells compared with that in the epicardial and endocardial cells.

Computer simulations. To understand why EAD developed from the epicardium under the acquired LQTS

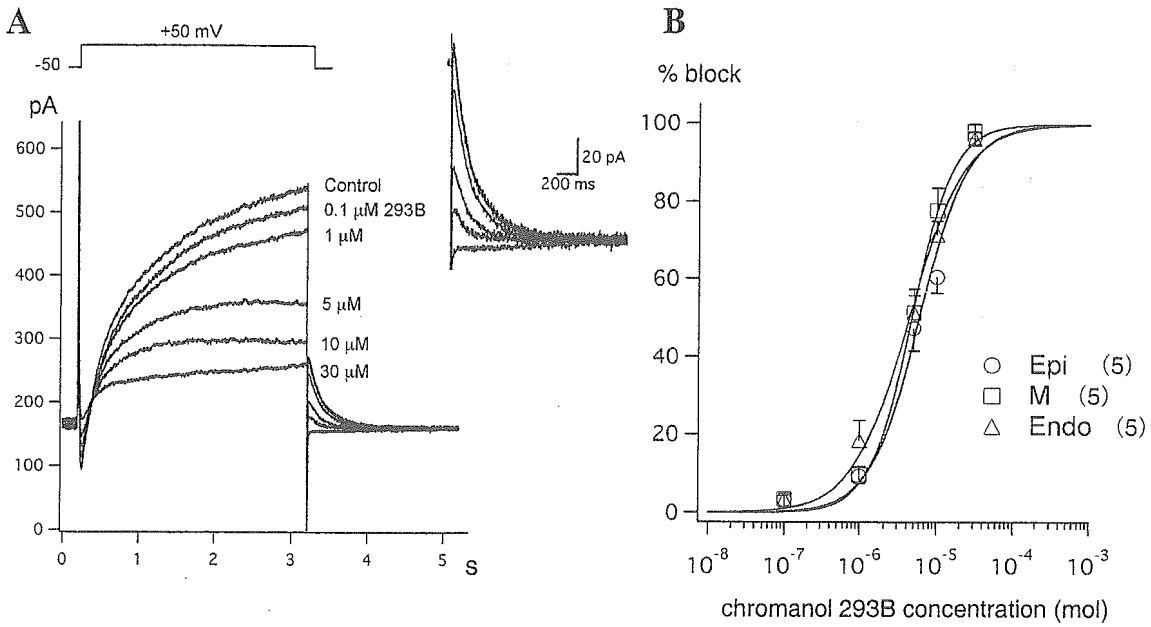

Figure 4. Sensitivity of I_{Ks} in the epicardial (Epi), midmyocardial (M), and endocardial (Endo) cells to inhibition by chromanol 293B. **(A)** Representative superimposed current traces elicited by 3-s depolarizing voltage-clamp steps applied from a holding potential of −50 mV to +50 mV in an epicardial cell, before (control) and during exposure to 293B at a concentration of 0.1, 1, 5, 10, and 30 μmol/l. The I_{Kr} inhibitor E-4031 (3 μmol/l) was present throughout. Tail currents were demonstrated on an expanded scale. **(B)** The percent block of I_{Ks} in the Epi **(open circles)**, M **(open squares)**, and Endo **(open triangles)** cells. The degree of I_{Ks} inhibition was measured as the fraction of the tail current reduced by each concentration of 293B with reference to the control amplitude of the tail current. **Smooth curves** through the data points represent a least-squares fit of a Hill equation: percent block = $100/(1 + (IC_{50}/[293B])^{nH})$, yielding the concentration required for the half-maximal block (IC_{50}) and the Hill coefficient (n_H). pA = pico (× 10^{-12}) Ampere.

condition, we simulated APs of the three cell types using a Luo-Rudy model at a BCL of 2,000 ms. As shown in Figure 6A, the epicardial APD was shorter than the M cells under the control condition (dotted line). However, suppression of both I_{Kr} and I_{Ks} (70% and 80%, respectively) (solid line), simulating the condition of acquired LQTS, developed EAD (arrow) from the epicardial cell but not from M or endocardial cells. Moreover, Figure 6B shows that the reactivation of Ca^{2+} current through the L-type channel ($I_{Ca,L}$) was responsible for the development of epicardial EAD under the acquired LQTS condition. Furthermore, a decrease in I_{to} density changed by G_{to} from 0.5 to 0.05

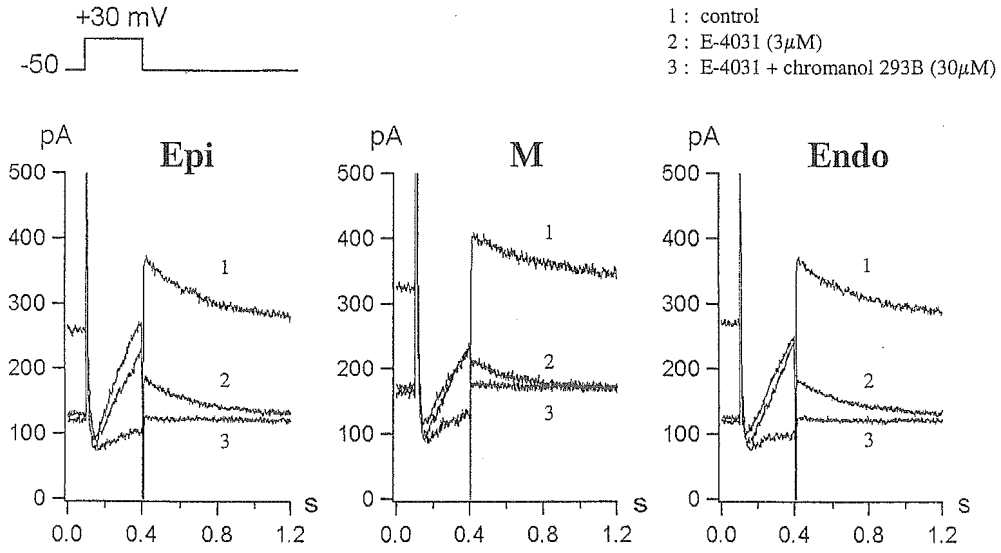

Figure 5. Detection of I_{Kr} and I_{Ks} in the epicardial (Epi), midmyocardial (M), and endocardial (Endo) cells. Depolarizing test pulses (to +30 mV for 300 ms) were repetitively applied (every 2 s) from a holding potential of −50 mV to activate I_K, and membrane currents were recorded from the Epi, M, and Endo cells, before (trace 1), and ~2 min after exposure to 3 μmol/l E-4031 (trace 2), and ~2 min after further addition of 30 μmol/l 293B in conjunction with 3 μmol/l E-4031 (trace 3). pA = pico (× 10^{-12}) Ampere.

Table 2. Transmural Heterogeneity of I_{Ks} and I_{Kr} in Feline Left Ventricle

	Epi (n = 10)	M (n = 9)	Endo (n = 7)
I_{Ks}	0.35 ± 0.26*	0.13 ± 0.09*†	0.30 ± 0.09*
I_{Kr}	1.34 ± 0.51	1.10 ± 0.38	1.17 ± 0.30

*$p < 0.05$ vs. I_{Kr}; †$p < 0.05$ vs. Epi and Endo by analysis of variance with Bonferroni's test. Mean ± SD, (pA/pF). Current densities of I_{Kr} and I_{Ks} measured as E-4031- and chromanol 293B-sensitive tail currents at −50 mV.
Abbreviations as in Table 1.

mS/μF decreased the net charge entry carried by the $I_{Ca,L}$ during the AP, resulted in suppressing EAD as well as abbreviating APD.

DISCUSSION

Genetic and ionic substrates of acquired LQTS. Acquired QT prolongation and TdP arrhythmias usually require multiple risk factors, such as bradycardia, hypokalemia, female gender, and mostly agents with an I_{Kr}-blocking effect. Recent genetic studies suggest some forms of acquired LQTS can be associated with silent mutations in the LQTS-related genes (4), such as *KCNQ1* encoding I_{Ks} (so-called forme fruste type of congenital LQTS) (5–7). Roden (20) hypothesized "reduced repolarization reserve" as a potential mechanism underlying susceptibility to drug-induced LQTS. According to his hypothesis, I_{Ks} dysfunction could be potentially compensated by other K^+ currents, mainly I_{Kr}, thereby the repolarization defect is tolerated, and agents with I_{Kr} block could induce acquired QT prolongation and TdP.

Vos et al. (21–23) suggested a high incidence of EADs and TdP by *d*-sotalol in dogs with chronic complete atrioventricular block as a result of a significant down-regulation of I_{Ks} and I_{Kr}. Moreover, other experimental studies using canine and rabbit wedge showed combined I_{Ks} and I_{Kr} block caused a high incidence of EADs most likely arising from the epicardium (14,15). Burashnikov and Antzelevitch (24) suggested that the abundant I_{Ks} in the epicardium and endocardium compared with the M region under normal conditions contributed to the increase in TDR but protected against development of EADs in the epicardium and endocardium in dogs. Thus, I_{Ks} is critically important for the repolarization reserve in the epicardium and endocardium.

Although I_{Ks} in the feline heart is far smaller than that in other species (25,26), our result from a whole-cell patch-clamp study suggested that a 10-μmol/l 293B used in the wedge preparation reduced about 70% of I_{Ks} in the three cell types, which is consistent with degree of I_{Ks} blockade caused by a silent mutation or common polymorphism in human *KCNQ1* gene (6,7). We also showed that I_{Kr} block with E-4031 in control conditions prolonged the QT interval but did not increase TDR and developed neither EADs nor TdP. However, combined I_{Kr} block with 293B further prolonged the QT interval and inverted T wave, which, in turn, increased TDR and induced EADs and TdP. There-

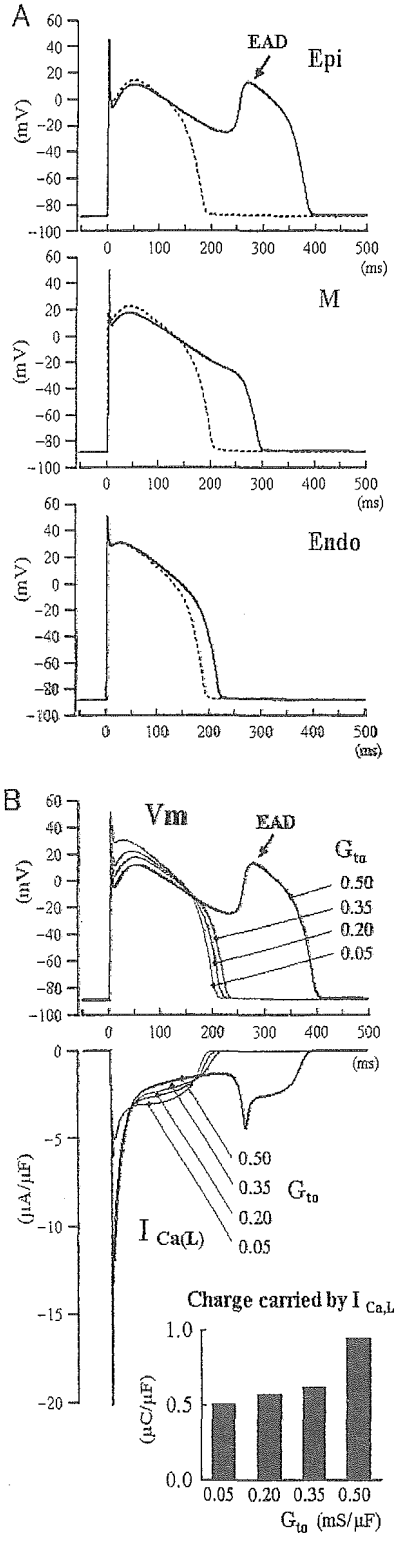

Figure 6. Effect of both I_{Kr} and I_{Ks} suppression on the simulated action potentials from the epicardial (Epi), midmyocardial (M), and endocardial (Endo) cells. **(A)** Superimposed action potentials simulated under baseline condition **(dotted lines)** and after both I_{Kr} and I_{Ks} suppression (70% and 80%, respectively) **(solid lines)**. **(B)** Effect of maximum conductance of I_{to} (G_{to}) on the simulated epicardial action potential (Vm), $I_{Ca,L}$ magnitude, and the net charge entry calculated by integration of the $I_{Ca,L}$ under the condition of both I_{Kr} and I_{Ks} suppression. Basic cycle length = 2,000 ms. EAD = early afterdepolarization.

fore, the feline heart is appropriate for a model of forme fruste LQTS. Our data also suggested that subclinical I_{Ks} dysfunction may become a genetic substrate, and additional I_{Kr} suppression may unmask marked QT prolongation and TdP in acquired form of LQTS.

Role of $I_{Ca,L}$ in increasing TDR and inducing EADs and TdP in acquired LQTS. Several clinical and experimental studies have suggested that EADs and triggered activity were important in the genesis of QT prolongation and TdP in LQTS (8,9,11–15,22–24). Induction of EADs generally requires an initiation or conditioning phase controlled by the sum of membrane currents present at the plateau AP (inward depolarization current and outward repolarization current). January and Riddle (27) suggested that the time- and voltage-dependent $I_{Ca,L}$ within its "window" was important in the induction and block of EADs. Luo and Rudy (28) suggested that EADs resulted from a secondary activation of the $I_{Ca,L}$ during the plateau of AP. However, the mechanism responsible for a high incidence of EADs (especially from the epicardium) and subsequent TdP under conditions of severely eliminated outward K^+ current, mimicking acquired LQTS, has not been mechanistically defined.

Our data indicate that accentuation of $I_{Ca,L}$ during the AP plateau preferentially prolonged APD and triggered EADs in the epicardium. This was based on the effect of verapamil on the epicardium. However, it is still unclear whether a larger $I_{Ca,L}$ in the epicardial cell compared with the M or endocardial cells contributed to the development of EADs. Recently, Bányász et al. (29) reported in their AP voltage clamp experiments that the epicardial cell had a pool of Ca^{2+} channels sufficient for a second activation, whereas the endocardial cells did not. Cordeiro et al. (30) also noted that the presence of spike-and-dome AP waveform in the epicardial cells resulted in a greater magnitude of $I_{Ca,L}$. Moreover, several simulation studies demonstrated a strong coupling between $I_{Ca,L}$ and I_{to} (31,32). Our simulation study also suggested that larger I_{to} in the epicardial cell caused larger $I_{Ca,L}$, developing EADs under the acquired LQTS condition. In the feline left ventricle, it has been reported that I_{to} is larger in the epicardium compared with the endocardium (33). Therefore, larger $I_{Ca,L}$ secondary to I_{to}-mediated spike-and-dome AP configuration in the epicardial cell might be responsible for the high incidence of EADs from the epicardium. This does not necessarily exclude the possible mechanisms of other ionic currents such as I_{NaCa} and Ca^{2+} release from sarcoplasmic reticulum, which may contribute to the prolonged AP as well as to the development of EADs under calcium-loading conditions (34).

Effects of catecholamines and verapamil in acquired LQTS. Treatment of drug-induced TdP begins with immediate withdrawal of any potential drugs and risk factors. Sanguinetti et al. (35) suggested that an increase of heart rate by isoproterenol was an effective therapeutic strategy in patients with acquired LQTS, because beta-adrenergic stimulation with isoproterenol abbreviates repolarization not only by increasing heart rate, but also by directly increasing the magnitude of I_{Ks}. However, our experimental data shows that epinephrine further prolonged APD in the epicardium and induced EADs and TdP probably due to augmentation of $I_{Ca,L}$ in the acquired LQTS condition. Thus, beta-adrenergic stimulation could be arrhythmogenic even in conditions of acquired LQTS when subclinical I_{Ks} dysfunction is present and heart rate is not fully increased.

Cosio et al. (8) used intravenous verapamil to treat three patients with TdP during an atrioventricular block. Shimizu et al. (9) reported that verapamil suppressed spontaneous or epinephrine-induced EADs and TdP in patients with congenital LQTS. Experimentally, Kimura et al. (36) reported that verapamil (2 μmol/l) suppressed cocaine-induced EADs in the myocytes isolated from feline left ventricle. Taken together with the data in the present study, $I_{Ca,L}$ block with verapamil may be a therapeutic choice for TdP in patients with acquired LQTS as well as congenital LQTS.

Study limitations. We assumed the activity recorded from the cut surface of the perfused wedge preparation represented cells within the respective layers of the wall throughout the wedge. Such validation was provided in previous studies that used the wedge preparation (10–15).

Pharmacologic block of I_{Ks} with 293B is not a complete surrogate for *KCNQ1* defect. However, our feline model closely mimicked the degree of I_{Ks} inhibition and pharmacologic features of acquired LQTS. Therefore, we believe these qualitative similarities validate 293B as a surrogate for forme fruste LQTS.

We simulated APs of the three cell types using a Luo-Rudy model, but it does not completely represent feline ventricular APs. However, the phenomenon that EAD frequently developed from the epicardium under the acquired LQTS condition was observed not only in cats but also in dogs and rabbits (14,15); thus, this simulation may support our speculation about the mechanism of this phenomenon.

Finally, the concentration of verapamil mainly used in this study (2.5 μmol/l = 1,250 ng/ml) was considerably higher than a typical clinical dose. However, verapamil was effective in suppressing EADs and decreasing TDR even at the lowest dose used in this study (0.1 μmol/l = 50 ng/ml), which is close to plasma concentration of verapamil after a 5-mg bolus injection (below 200 ng/ml).

Acknowledgments

The authors thank Drs. Charles Antzelevitch and Masahiko Kondo for their helpful suggestions and technical instructions, and Drs. Hans-J. Lang and Jürgen Pünter (Aventis Pharma Deutschland GmbH, Frankfurt, Germany) for kindly providing the chromanol 293B.

Reprint requests and correspondence: Dr. Wataru Shimizu, Division of Cardiology, Department of Internal Medicine, National Cardiovascular Center, 5-7-1 Fujishiro-dai, Suita, Osaka, 565-8565 Japan. E-mail: wshimizu@hsp.ncvc.go.jp.

REFERENCES

1. Schwartz PJ, Periti M, Malliani A. The long Q-T syndrome. Am Heart J 1975;89:378–90.
2. Moss AJ, Schwartz PJ, Crampton RS, et al. The long QT syndrome: prospective longitudinal study of 328 families. Circulation 1991;84: 1136–44.
3. Roden DM, Lazzara R, Rosen M, et al. Multiple mechanisms in the long-QT syndrome: current knowledge, gaps and future directions. Circulation 1996;94:1996–2012.
4. Yang P, Kanki H, Drolet B, et al. Allelic variants in long-QT disease genes in patients with drug-associated Torsades de Pointes. Circulation 2002;105:1943–8.
5. Donger C, Denjoy I, Berthet M, et al. KVLQT1 c-terminal missense mutation causes a forme fruste long-QT syndrome. Circulation 1997;96:2778–81.
6. Napolitano C, Schwartz PJ, Brown AM, et al. Evidence for a cardiac ion channel mutation underlying drug-induced QT prolongation and life-threatening arrhythmias. J Cardiovasc Electrophysiol 2000;11: 691–6.
7. Kubota T, Shimizu W, Kamakura S, et al. Hypokalemia-induced long QT syndrome with underlying novel missense mutation in S4-S5 linker of KCNQ1. J Cardiovasc Electrophysiol 2000;11:1048–54.
8. Cosio FG, Goicolea A, López-Gil L, Kallmeier C, Barroso L. Suppression of Torsades de Pointes with verapamil in patients with atrio-ventricular block. Eur Heart J 1991;12:635–8.
9. Shimizu W, Ohe T, Kurita T, et al. Effects of verapamil and propranolol on early afterdepolarizations and ventricular arrhythmias induced by epinephrine in congenital long QT syndrome. J Am Coll Cardiol 1995;26:1299–309.
10. Aiba T, Shimizu W, Inagaki M, et al. Transmural heterogeneity of the action potential configuration in the feline left ventricle. Circ J 2003;67:449–54.
11. Antzelevitch C, Sun ZQ, Zhang ZQ, Yan GX. Cellular and ionic mechanisms underlying erythromycin-induced long QT intervals and Torsade de Pointes. J Am Coll Cardiol 1996;28:1836–48.
12. Shimizu W, Antzelevitch C. Sodium channel block with mexiletine is effective in reducing transmural dispersion of repolarization and preventing Torsade de Pointes in LQT2 and LQT3 models of the long-QT syndrome. Circulation 1997;96:2038–47.
13. Shimizu W, Antzelevitch C. Effects of a K^+ channel opener to reduce transmural dispersion of repolarization and prevent Torsade de Pointes in LQT1, LQT2, and LQT3 models of the long-QT syndrome. Circulation 2000;102:706–12.
14. Emori T, Antzelevitch C. Cellular basis for complex T wave and arrhythmic activity following combined I_{Kr} and I_{Ks} block. J Cardiovasc Electrophysiol 2001;12:1369–78.
15. Yan GX, Wu Y, Liu T, et al. Phase 2 early afterdepolarization as a trigger of polymorphic ventricular tachycardia in acquired long-QT syndrome, direct evidence from intracellular recordings in the intact left ventricular wall. Circulation 2001;103:2851–6.
16. Hamill OP, Marty A, Neher E, Sakmann B, Sigworth FJ. Improved patch-clamp techniques for high-resolution current recording from cells and cell-free membrane patches. Pflügers Arch 1981;391:85–100.
17. Benitah JP, Gomez AM, Bailly P, et al. Heterogeneity of the early outward current in ventricular cells isolated from normal and hypertrophied rat hearts. J Physiol 1993;469:111–38.
18. Clancy CE, Rudy Y. Na^+ channel mutation that causes both Brugada and long-QT syndrome phenotypes, a simulation study of mechanism. Circulation 2002;105:1208–13.
19. Dumaine R, Towbin JA, Brugada P, et al. Ionic mechanisms responsible for the electrocardiographic phenotype of the Brugada syndrome are temperature dependent. Circ Res 1999;85:803–9.
20. Roden DM. Taking the "idio" out of "idiosyncratic": predicting Torsades de Pointes. Pacing Clin Electrophysiol 1998;21:1029–34.
21. Vos MA, Verduyn SC, Gorgels APM, et al. Reproducible induction of early afterdepolarizations and Torsade de Pointes arrhythmias by d-sotalol and pacing in dogs with chronic atrioventricular block. Circulation 1995;91:864–72.
22. Vos MA, Groot SHM, Verduyn SC, et al. Enhanced susceptibility for acquired Torsade de Pointes arrhythmias in the dog with chronic, complete AV block is related to cardiac hypertrophy and electrical remodeling. Circulation 1998;98:1125–35.
23. Volders PGA, Sipido KR, Vos MA, et al. Downregulation of delayed rectifier K^+ currents in dogs with chronic complete atrioventricular block and acquired Torsades de Pointes. Circulation 1999;100:2455–61.
24. Burashnikov A, Antzelevitch C. Prominent I_{Ks} in epicardium and endocardium contributes to development of transmural dispersion of repolarization but protects against development of early afterdepolarizations. J Cardiovasc Electrophysiol 2002;13:172–7.
25. Follmer CH, Colatsky TJ. Block of delayed rectifier potassium current, I_K, by flecainide and E-4031 in cat ventricular myocytes. Circulation 1990;82:289–93.
26. Martínez HB, Elizalde A, Chapula JS. Developmental differences in delayed rectifying outward current in feline ventricular myocytes. Am J Physiol 2000;278:H484–92.
27. January CT, Riddle JM. Early afterdepolarizations: mechanism of induction and block, a role for L-type Ca^{2+} current. Circ Res 1989;64:977–90.
28. Luo CH, Rudy Y. A dynamic model of the cardiac ventricular action potential II afterdepolarizations, triggered activity, and potentiation. Circ Res 1994;74:1097–113.
29. Bányász T, Fülöp L, Magyar J, et al. Endocardial versus epicardial differences in L-type calcium current in canine ventricular myocytes studied by action potential voltage clamp. Cardiovasc Res 2003;58: 66–75.
30. Cordeiro JM, Greene L, Heilmann C, Antzelevitch D, Antzelevitch C. Transmural heterogeneity of calcium activity and mechanical function in the canine left ventricle. Am J Physiol 2004;286:H1471–9.
31. Greenstein JL, Wu R, Po S, et al. Role of the calcium-independent transient outward current Ito1 in shaping action potential morphology and duration. Cir Res 2000;87:1026–33.
32. Miyoshi S, Mitamura H, Fujikawa K, et al. A mathematical model of phase 2 reentry: role of L-type Ca current. Am J Physiol 2003;284: H1285–94.
33. Furukawa T, Myerburg RJ, Furukawa N, et al. Differences in transient outward currents of feline endocardial and epicardial myocytes. Circ Res 1990;67:1287–91.
34. Zygmunt AC, Goodrow RJ, Antzelevitch C. I_{NaCa} contributes to electrical heterogeneity within the canine ventricle. Am J Physiol 2000;278:H1671–8.
35. Sanguinetti MC, Jurkiewicz NK, Scott A, Siegl PKS. Isoproterenol antagonizes prolongation of refractory period by class III antiarrhythmic agent E-4031 in guinea pig myocytes, mechanism of action. Circ Res 1991;68:77–84.
36. Kimura S, Bassett AL, Xi H, Myerburg RJ. Early afterdepolarizations and triggered activity induced by cocaine, a possible mechanism of cocaine arrhythmogenesis. Circulation 1992;85:2227–35.

Acta Physiol Scand 2005, 184, 187–193

Myocardial interstitial choline and glutamate levels during acute myocardial ischaemia and local ouabain administration

T. Kawada,[1] T. Yamazaki,[2] T. Akiyama,[2] T. Shishido,[1] H. Mori[2] and M. Sugimachi[1]

1 *Department of Cardiovascular Dynamics, National Cardiovascular Center Research Institute, Osaka, Japan*

2 *Department of Cardiac Physiology, National Cardiovascular Center Research Institute, Osaka, Japan*

Received 25 November 2004, accepted 16 March 2005
Correspondence: T. Kawada, Department of Cardiovascular Dynamics, National Cardiovascular Center Research Institute, 5-7-1 Fujishirodai, Suita, Osaka 565-8565, Japan.
E-mail: torukawa@res.ncvc.go.jp

Abstract

Aim: Noradrenaline (NA) uptake transporters are known to reverse their action during acute myocardial ischaemia and to contribute to ischaemia-induced myocardial interstitial NA release. By contrast, functional roles of choline and glutamate transporters during acute myocardial ischaemia remain to be investigated. Because both transporters are driven by the normal Na^+ gradient across the plasma membrane in a similar manner to NA transporters, the loss of Na^+ gradient would affect the transporter function, which would in turn alter myocardial interstitial choline and glutamate levels. The aim of the present study was to examine the effects of acute myocardial ischaemia and the inhibition of Na^+,K^+-ATPase on myocardial interstitial glutamate and choline levels.

Methods: In anaesthetized cats, we measured myocardial interstitial glutamate and choline levels while inducing acute myocardial ischaemia or inhibiting Na^+,K^+-ATPase by local administration of ouabain.

Results: The choline level was not changed significantly by ischaemia (from 0.93 ± 0.06 to 0.82 ± 0.13 μM, mean $\pm$ SE, $n = 6$) and was decreased slightly by ouabain (from 1.30 ± 0.06 to 1.05 ± 0.07 μM, $P < 0.05$, $n = 6$). The glutamate level was significantly increased from 9.5 ± 1.9 to 34.7 ± 6.1 μM by ischaemia ($P < 0.01$, $n = 6$) and from 8.9 ± 1.0 to 15.9 ± 2.3 μM by ouabain ($P < 0.05$, $n = 6$). Inhibition of glutamate transport by *trans*-L-pyrrolidine-2,4-dicarboxylate (*t*-PDC) suppressed ischaemia- and ouabain-induced glutamate release.

Conclusion: Myocardial interstitial choline level was not increased by acute myocardial ischaemia or by Na^+,K^+-ATPase inhibition. By contrast, myocardial interstitial glutamate level was increased by both interventions. The glutamate transporter contributed to glutamate release via retrograde transport.

Keywords acetylcholine, cardiac microdialysis, cats, coronary artery occlusion, myocardium, noradrenaline.

Acute myocardial ischaemia causes oxygen depletion and loss of ATP in the ischaemic region (Hearse 1979). Blockade of H^+-ATPase leads to noradrenaline (NA) leakage from storage vesicles and axoplasmic NA accumulation (Schömig *et al.* 1988). Intracellular acidosis causes Na^+ influx via Na^+/H^+ exchange. Inhibition of Na^+,K^+-ATPase activity reduces the Na^+ gradient across the plasma membrane. Because NA uptake transporters are driven by the normal Na^+ electrochemical gradient across the plasma membrane,

axoplasmic NA accumulation and reduction of the Na^+ gradient cause reverse transport of NA from the intracellular space to the extracellular space (Schwartz 2000). Acute myocardial ischaemia evokes the myocardial interstitial NA release in the ischaemic region via retrograde NA transport, independently of efferent sympathetic nerve activity (Schömig *et al.* 1984, Yamazaki *et al.* 1996, Akiyama & Yamazaki 1999, Kawada *et al.* 2001a).

Similar to NA, choline and glutamate are taken up into cells by plasma membrane transporters driven by the Na^+ gradient (Schwartz 2000). We hypothesized that the loss of Na^+ gradient under ischaemic conditions would interfere with the transporter function, which would in turn alter myocardial interstitial choline and glutamate levels. Choline release has been suggested as an index of ischaemic degradation of the myocardial phospholipid bilayer in isolated, Tyrode solution-perfused rat hearts (Brühl *et al.* 2004). Glutamate can be a preferred myocardial fuel during ischaemia and may have protective effects on ischaemic myocardium (Arsenian 1998). Measuring myocardial interstitial levels of these molecules *in vivo* would contribute to understanding the pathophysiology of acute myocardial ischaemia. To test the hypothesis, we employed an *in vivo* cardiac microdialysis technique and measured myocardial interstitial choline and glutamate levels in anaesthetized cats (Akiyama *et al.* 1991, 1994, Yamazaki *et al.* 1997, Kawada *et al.* 2001b). Acute myocardial ischaemia inevitably affects systemic haemodynamics and perfusion of the heart. To minimize such haemodynamic effects, we also examined the effects of Na^+,K^+-ATPase inhibition on the myocardial interstitial choline and glutamate levels by locally administering ouabain through a dialysis probe (Yamazaki *et al.* 1999, Kawada *et al.* 2002). The results of the present study indicated that the myocardial interstitial choline level was not increased by acute myocardial ischaemia or by Na^+,K^+-ATPase inhibition. By contrast, the myocardial interstitial glutamate level was increased by both interventions. The glutamate transporter contributed to glutamate release via retrograde transport.

Materials and methods

Surgical preparation

Animal care was conducted in strict accordance with the *Guiding Principles for the Care and Use of Animals in the Field of Physiological Sciences* approved by the Physiological Society of Japan. Adult cats weighing 2.0–4.8 kg were anaesthetized via an intraperitoneal injection of pentobarbital sodium (30–35 mg kg^{-1}) and ventilated mechanically with room air mixed with oxygen. The depth of anaesthesia was maintained with a continuous intravenous infusion of pentobarbital sodium (1–2 mg kg^{-1} h^{-1}) through a catheter inserted via the right femoral vein. Mean systemic arterial pressure was monitored from a catheter inserted via the right femoral artery.

With the animal in the lateral position, the left fifth and sixth ribs were resected to expose the heart. When a coronary occlusion was necessary, a 3-0 silk suture was prepared around the left anterior descending coronary artery (LAD) just distal to the first diagonal branch. With a fine guiding needle, a dialysis probe was implanted into the left ventricular free wall perfused by the LAD. Heparin sodium (100 U kg^{-1} bolus injection followed by a maintenance dose of 50 U kg^{-1} h^{-1}) was administered intravenously to prevent blood coagulation. At the end of the experiment the experimental animals were killed by an overdose of pentobarbital sodium. We confirmed that the dialysis probe had been implanted within the left ventricular myocardium.

Dialysis technique

We designed a transverse dialysis probe (Akiyama *et al.* 1991, 1994). For measurements of small molecular compounds including ACh, choline, and glutamate, we used a dialysis fibre of 50 000 molecular weight cutoff (13 mm length, 310 μm OD, 200 μm ID; PAN-1200, Asahi Chemical, Osaka, Japan) with both ends glued to polyethylene tubes (20 cm length, 500 μm OD, 200 μm ID). The dialysis probe was perfused at a rate of 2 μL min^{-1} with Ringer solution. Each sample was collected in a microtube containing 3 μL of phosphate buffer (100 mM, pH 3.5). A cholinesterase inhibitor eserine (100 μM) was added to the perfusate to measure ACh. A preliminary examination indicated that whether the perfusate-contained eserine did not affect myocardial interstitial choline levels significantly. Dead space volume between the dialysis fibre and the sample microtube was identical for ACh, choline, and glutamate measurements, and the sampling was performed taking into account the time for dialysate to traverse the dead space volume.

The dialysate ACh and choline levels were measured directly by high-performance liquid chromatography with electrochemical detection. The absolute detection limits of ACh and choline, determined with a signal-to-noise ratio of 3, were 10 and 5 fmol per injection, respectively. The dialysate glutamate level was measured by kinetic enzymatic analysis with CMA 600. The absolute detection limit of glutamate was 1 μM per injection.

Protocols

All protocols were started from 2 h after implanting the dialysis probe. To examine changes in myocardial

interstitial ACh and choline levels during acute myocardial ischaemia ($n = 6$), after collecting a 15-min baseline dialysate sample, we occluded the LAD for 60 min and obtained four consecutive 15-min dialysate samples. The full-length of the implanted dialysis fibre was located within the ischaemic area judged by discolouration of myocardium during the LAD occlusion. We then released the occlusion and collected a 15-min dialysate sample during reperfusion. To examine changes in myocardial ACh and choline levels in response to local ouabain administration ($n = 6$), after collecting a 15-min baseline dialysate sample, we replaced the perfusate with Ringer solution containing 100 μM ouabain and collected four consecutive 15-min dialysate samples.

In different groups of animals, myocardial interstitial glutamate levels were measured during acute myocardial ischaemia ($n = 6$) and during local administration of ouabain ($n = 6$). To elucidate the role of the glutamate transporter, we also examined the effects of glutamate transport inhibition by *trans*-L-pyrrolidine-2,4-dicarboxylate (*t*-PDC, 10 mM) on myocardial interstitial glutamate levels during acute myocardial ischaemia ($n = 7$) and local administration of ouabain ($n = 7$). *t*-PDC was locally administered through the dialysis probe to avoid systemic effects.

Statistical analysis

All data are presented as mean ± SE values. In each protocol, the effects of myocardial ischaemia or local ouabain administration were examined using one-way analysis of variance followed by Dunnett's test against the corresponding baseline level (Glantz 2002). The baseline as well as maximum glutamate levels with and without glutamate transport inhibition were compared by an unpaired *t*-test during acute myocardial ischaemia or during local ouabain administration (Glantz 2002). Differences were considered to be significant when $P < 0.05$.

Results

Figure 1a shows myocardial interstitial ACh level during acute myocardial ischaemia. The ACh level was increased by LAD occlusion, becoming approximately 15 times higher than the baseline level at 30–45 and 45–60 min of ischaemia. The ACh level decreased towards the baseline level upon reperfusion. Figure 1b illustrates myocardial interstitial choline level during acute myocardial ischaemia. The choline level did not change significantly throughout the ischaemic and reperfusion periods.

Figure 2a shows changes in myocardial interstitial ACh level during local administration of ouabain. The ACh level was increased by the inhibition of

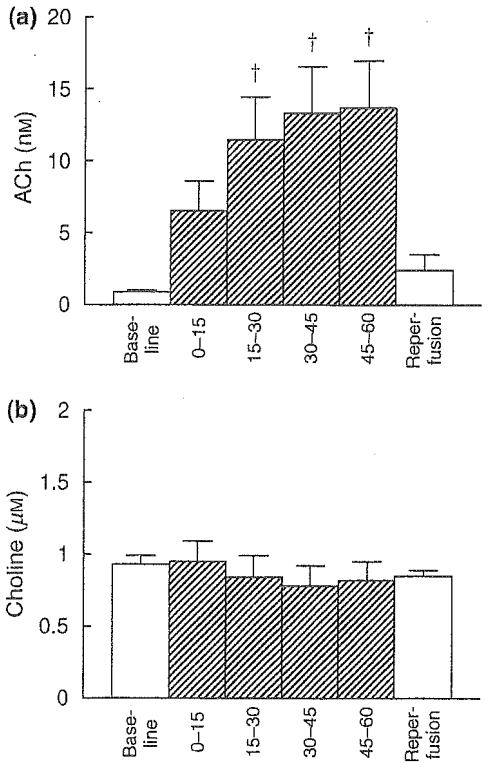

Figure 1 Changes in myocardial interstitial acetylcholine (ACh) level (a) and choline level (b) during coronary artery occlusion and reperfusion. Myocardial interstitial ACh level was significantly increased by acute myocardial ischaemia, while myocardial interstitial choline level was not changed. Data are mean ± SE. †$P < 0.01$ from baseline.

Na^+,K^+-ATPase, becoming approximately nine times higher than the baseline level at 15–30 min. The ACh level then decreased but remained significantly higher than the baseline level. Figure 2b illustrates the myocardial interstitial choline level during local administration of ouabain. The choline level was significantly lower at 0–15 and 45–60 min when compared with the baseline level.

Figure 3a shows changes in myocardial interstitial glutamate level during acute myocardial ischaemia. LAD occlusion increased the glutamate level to approximately 3.5 times higher than the baseline level at 0–15 min. Thereafter, the glutamate level was significantly higher than the baseline level throughout the ischaemic and reperfusion periods. Figure 3b illustrates the effects of glutamate transport inhibition on the ischaemia-induced glutamate release. The baseline glutamate level was significantly decreased by glutamate transport inhibition ($P < 0.05$). Although acute myocardial ischaemia and reperfusion significantly increased the glutamate level relative to the baseline level, the maximum glutamate level was attenuated to approximately one-fifth compared with that observed without glutamate transport inhibition ($P < 0.05$).

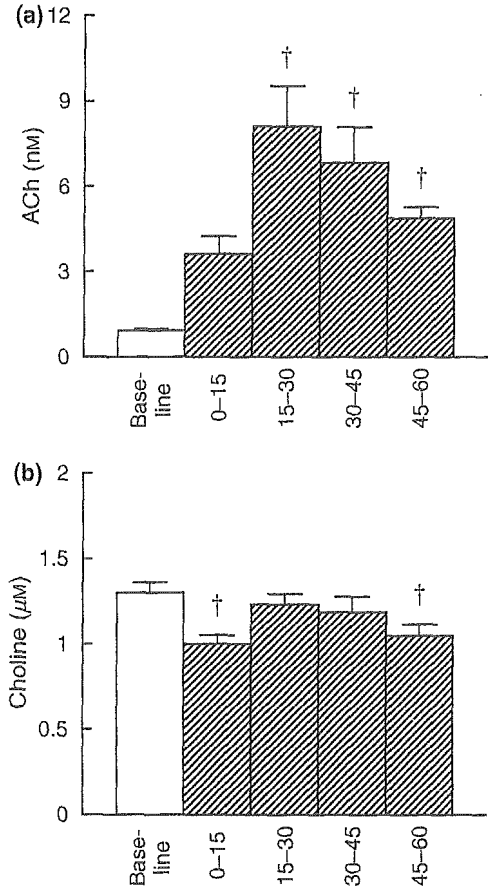

Figure 2 Changes in myocardial interstitial acetylcholine (ACh) level (a) and choline level (b) in response to the local administration of ouabain. Myocardial interstitial ACh level was significantly increased by ouabain. In contrast, myocardial interstitial choline level was decreased by ouabain. Data are mean ± SE. †$P < 0.01$ from baseline.

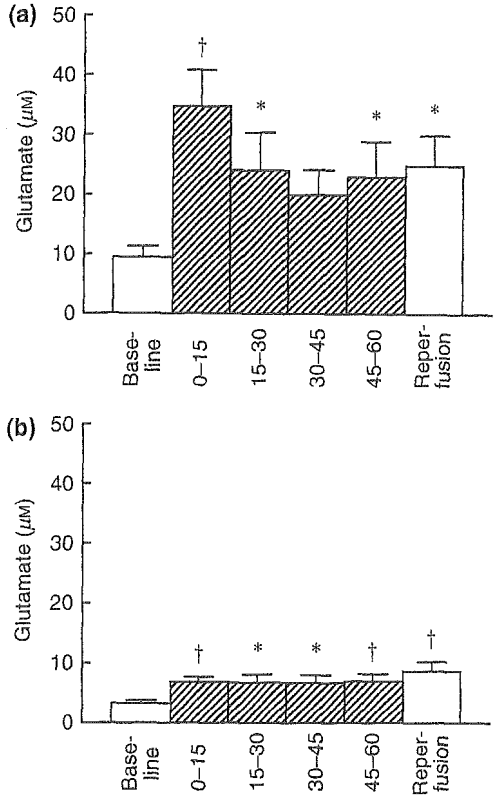

Figure 3 Changes in myocardial interstitial glutamate level during coronary artery occlusion and reperfusion without (a) and with (b) the inhibition of glutamate transporter. The glutamate level was significantly increased by acute myocardial ischaemia. The ischaemia-induced glutamate release was suppressed by the inhibition of glutamate transporter. Data are mean ± SE. †$P < 0.01$ and *$P < 0.05$ from baseline.

Figure 4a shows changes in myocardial interstitial glutamate level during the local administration of ouabain. Ouabain administration did not change the glutamate level at 0–15 min but increased the glutamate level thereafter. The glutamate level became approximately 1.8 times higher than the baseline level at 30–45 min. Figure 4b illustrates the effects of glutamate transport inhibition on ouabain-induced glutamate release. The baseline glutamate level was significantly decreased by the inhibition of glutamate transport ($P < 0.05$). Although ouabain administration increased the glutamate level relative to the baseline level, the maximum glutamate level was suppressed to approximately one-third of that observed without glutamate transport inhibition ($P < 0.05$).

Discussion

We have shown that acute myocardial ischaemia and local inhibition of Na^+,K^+-ATPase increased myocardial interstitial glutamate level but not choline level. Despite the similar Na^+ gradient dependency of corresponding transporters, myocardial interstitial glutamate and choline levels showed differential responses to the two interventions.

Changes in myocardial interstitial choline level

In the vagal nerve endings, ACh is hydrolysed to acetate and choline by acetylcholinesterase (Nicholls 1994). Choline is then taken up into the vagal nerve endings by the choline transporter driven by the Na^+ gradient. We hypothesized that loss of Na^+ gradient during acute myocardial ischaemia or local ouabain administration would increase the myocardial interstitial choline level by the interruption of choline uptake. Contrary to our hypothesis, acute myocardial ischaemia did not change myocardial interstitial choline level in the ischaemic region (Fig. 1b). Ouabain administration decreased the myocardial interstitial choline level at 0–15 and 45–60 min (Fig. 2b).

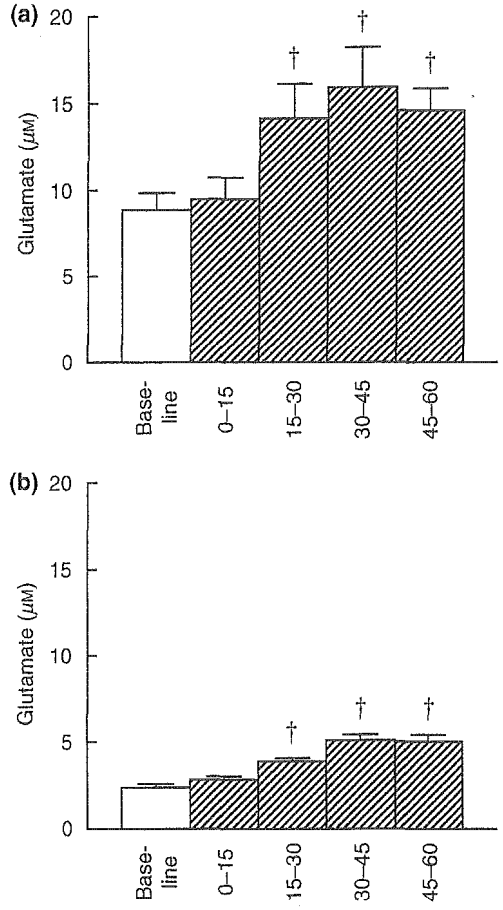

Figure 4 Changes in myocardial interstitial glutamate level in response to the local administration of ouabain without (a) and with (b) the inhibition of glutamate transporter. The glutamate level was significantly increased by ouabain administration. The ouabain-induced glutamate release was suppressed by the inhibition of glutamate transporter. Data are mean ± SE. †$P < 0.01$ from baseline.

Possible explanations for the absence of ischaemia- or ouabain-induced choline release are as follows. First, choline uptake is the rate-limiting step for ACh synthesis (Lockman & Allen 2002). Because choline in the intracellular space is rapidly consumed for ACh synthesis, the axoplasmic choline concentration might have been too low to evoke reverse transport by the choline transporter. Second, plasma choline concentration is stabilized by *de novo* choline synthesis from the catabolism of phosphatidylcholine found in cell membranes (Lockman & Allen 2002). Potential choline release may have been counterbalanced by the local stabilization mechanisms. Taking into account the recovery rate of the dialysis probe (approximately 30%), the myocardial interstitial choline concentration was 3–5 μM. Although the estimated concentration was lower than the highly regulated plasma choline concentration of approximately 10 μM, it was much higher than the ischaemia-induced maximum choline release (approximately 0.6 μM) in isolated rat hearts reported by Brühl *et al.* (2004). The present results suggest that myocardial interstitial choline level may not serve as an indicator of myocardial ischaemia in blood-perfused *in vivo* feline hearts.

By contrast with myocardial interstitial choline level, myocardial interstitial ACh level was increased both by acute myocardial ischaemia and by local administration of ouabain. Because ischaemia-induced ACh release was observed after vagal nerve transection in a previous study (Kawada *et al.* 2000), a Ca^{2+} channel-independent, regional release mechanism appears to be involved. Several reports have suggested that ouabain or ischaemia-induced intracellular Na^+ accumulation could elevate intracellular Ca^{2+} level via Na^+/Ca^{2+} exchange (Mochizuki & Jiang 1998, Li *et al.* 2000). The elevation of intracellular Ca^{2+} level may be associated with ACh release. Our previous study indicated that intracellular Ca^{2+} overload due to Ca^{2+} mobilization is responsible for the ACh release evoked by ischaemia (Kawada *et al.* 2000).

Changes in myocardial interstitial glutamate levels

Although the glutamate transporter family differs from the NA transporter family in that it requires counter-transport of K^+ instead of cotransport of Cl^-, its primary driving force is the Na^+ gradient across the plasma membrane (Schwartz 2000). Therefore, interventions that reduce the Na^+ gradient are likely to cause reverse transport of glutamate, in a similar manner to the reverse transport of NA. Acute myocardial ischaemia increased the myocardial interstitial glutamate level (Fig. 3a) as consistent with previous reports (Kennergren *et al.* 1997, 1999, Bäckström *et al.* 2003, Song *et al.* 1996). Inhibition of Na^+,K^+-ATPase also induced myocardial interstitial glutamate release (Fig. 4a). Glutamate release during acute myocardial ischaemia and local ouabain administration was significantly attenuated by the inhibition of glutamate transport (Figs 3b and 4b), suggesting the involvement of reverse transport by the glutamate transporter. Glutamate plays a vital role in keeping nitrogen balance in cells as a common amino acid in transamination reactions. The high intra-to-extracellular concentration ratio of glutamate would contribute to the retrograde transport by the glutamate transporter during the loss of normal Na^+ gradient.

In the case of myocardial interstitial NA levels, local blockade of NA uptake increased baseline NA levels, suggesting the accumulation of NA spontaneously released into the synaptic cleft (Akiyama & Yamazaki 1999). We therefore predicted that the inhibition of glutamate transport would increase the baseline gluta-

mate level. However, the inhibition of glutamate transport actually decreased the baseline glutamate level (Figs 3 and 4), suggesting that spontaneous glutamate release rather than glutamate uptake had occurred under baseline conditions. The insertion of a dialysis probe inevitably damages the myocardium. Although we waited for 2 h after implantation of the dialysis probe and the glutamate level declined with time, glutamate release from damaged myocardium may have continued. Notwithstanding this limitation, we were able to detect glutamate release in response to acute myocardial ischaemia and inhibition of Na^+,K^+-ATPase. Therefore, our interpretation that glutamate release was dependent on the reverse transport of glutamate transporter may be reasonable.

Supplementing the heart with glutamate has been shown to have beneficial effect on the recovery of contractile function in post-surgical patients (Arsenian 1998). The myocardial interstitial glutamate level remained increased during 15-min reperfusion whereas the myocardial interstitial ACh level returned towards the baseline level. Although the reason for different responses upon reperfusion was unanswered in the present study, the sustained increase in the glutamate level may have therapeutic effect on its own.

In conclusion, acute myocardial ischaemia and inhibition of Na^+,K^+-ATPase did not increase myocardial interstitial choline level despite a significant increase in myocardial interstitial ACh level. By contrast, both interventions significantly increased the myocardial interstitial glutamate level. The glutamate transporter contributed to myocardial interstitial glutamate release via retrograde transport.

This study was supported by Health and Labour Sciences Research Grant for Research on Advanced Medical Technology (H14-Nano-002) from the Ministry of Health Labour and Welfare of Japan, by Grant-in-Aid for Scientific Research (C-15590786) from the Ministry of Education, Science, Sports and Culture of Japan, and by the Program for Promotion of Fundamental Studies in Health Science of the Organization for Pharmaceutical Safety and Research from Pharmaceuticals and Medical Devices Agency (PMDA).

References

Akiyama, T. & Yamazaki, T. 1999. Norepinephrine release from cardiac sympathetic nerve endings in the in vivo ischemic region. *J Cardiovasc Pharmacol* 34(Suppl. 4), S11–S14.

Akiyama, T., Yamazaki, T. & Ninomiya, I. 1991. In vivo monitoring of myocardial interstitial norepinephrine by dialysis technique. *Am J Physiol Heart Circ Physiol* 261, H1643–H1647.

Akiyama, T., Yamazaki, T. & Ninomiya, I. 1994. In vivo detection of endogenous acetylcholine release in cat ventricles. *Am J Physiol Heart Circ Physiol* 266, H854–H860.

Arsenian, M. 1998. Potential cardiovascular applications of glutamate, aspartate, and other amino acids. *Clin Cardiol* 21, 620–624.

Bäckström, T., Goiny, M., Lockowandt, U., Liska, J. & Franco-Cereceda, A. 2003. Cardiac outflow of amino acids and purines during myocardial ischemia and reperfusion. *J Appl Physiol* 94, 1122–1128.

Brühl, A., Hafner, G. & Löffelholz, K. 2004. Release of choline in the isolated heart, an indicator of ischemic phospholipid degradation and its protection by ischemic preconditioning: no evidence for a role of phospholipase D. *Life Sci* 75, 1609–1620.

Glantz, S.A. 2002. *Primer of Biostatistics*, 5th edn. McGraw-Hill, New York.

Hearse, D.J. 1979. Oxygen deprivation and early myocardial contractile failure: a reassessment of the possible role of adenosine triphosphate. *Am J Cardiol* 44, 1115–1121.

Kawada, T., Yamazaki, T., Akiyama, T. *et al.* 2000. Differential acetylcholine release mechanisms in the ischemic and non-ischemic myocardium. *J Mol Cell Cardiol* 32, 405–414.

Kawada, T., Yamazaki, T., Akiyama, T. *et al.* 2001a. Vagosympathetic interactions in ischemia-induced myocardial norepinephrine and acetylcholine release. *Am J Physiol Heart Circ Physiol* 280, H216–H221.

Kawada, T., Yamazaki, T., Akiyama, T. *et al.* 2001b. In vivo assessment of acetylcholine-releasing function at cardiac vagal nerve terminals. *Am J Physiol Heart Circ Physiol* 281, H139–H145.

Kawada, T., Yamazaki, T., Akiyama, T. *et al.* 2002. Disruption of vagal efferent axon and nerve terminal function in the postischemic myocardium. *Am J Physiol Heart Circ Physiol* 283, H2687–H2691.

Kennergren, C., Nyström, B., Nyström, U. *et al.* 1997. In situ detection of myocardial infarction in pig by measurements of aspartate aminotransferase (ASAT) activity in the interstitial fluid. *Scand Cardiovasc J* 31, 343–349.

Kennergren, C., Mantovani, V., Lönnroth, P., Nyström, B., Berglin, E. & Hamberger, A. 1999. Extracellular amino acids as markers of myocardial ischemia during cardioplegic heart arrest. *Cardiology* 91, 31–40.

Li, S., Jiang, Q., Stys, P.K. 2000. Important role of reverse Na^+-Ca^{2+} exchange in spinal cord white matter injury at physiological temperature. *J Neurophysiol* 84, 1116–1119.

Lockman, P.R. & Allen, D.D. 2002. The transport of choline. *Drug Dev Ind Pharm* 28, 749–771.

Mochizuki, S. & Jiang, C. 1998. Na^+/Ca^{++} exchanger and myocardial ischemia/reperfusion. *Jpn Heart J* 39, 707–714.

Nicholls, D.G. 1994. *Proteins, Transmitters and Synapses*, pp. 186–199. Blackwell Science, London.

Schömig, A., Dart, A.M., Dietz, R., Mayer, E. & Kübler, W. 1984. Release of endogenous catecholamines in the ischemic myocardium of the rat. Part A: Locally mediated release. *Circ Res* 55, 689–701.

Schömig, A., Kurz, T., Richardt, G. & Schömig, E. 1988. Neuronal sodium homeostasis and axoplasmic amine concentration determine calcium-independent noradrenaline release in normoxic and ischemic rat heart. *Circ Res* 63, 214–226.

Schwartz, J.H. 2000. Neurotransmitters. In: E.R. Kandel, J.H. Schwartz & T.M. Jessell (eds) *Principles of Neural Science*, 4th edn, pp. 280–297. McGraw-Hill, New York.

Song, D., O'Regan, M.H. & Phillis, J.W. 1996. Release of the excitotoxic amino acids, glutamate and aspartate, from the isolated ischemic/anoxic rat heart. *Neurosci Lett* 220, 1–4.

Yamazaki, T., Akiyama, T., Kitagawa, H., Takauchi, Y. & Kawada, T. 1996. Elevation of either axoplasmic norepinephrine or sodium level induced release of norepinephrine from cardiac sympathetic nerve terminals. *Brain Res* 737, 343–346.

Yamazaki, T., Akiyama, T., Kitagawa, H., Takauchi, Y., Kawada, T. & Sunagawa, K. 1997. A new, concise dialysis approach to assessment of cardiac sympathetic nerve terminal abnormalities. *Am J Physiol Heart Circ Physiol* 272, H1182–H1187.

Yamazaki, T., Akiyama, T. & Kawada, T. 1999. Effects of ouabain on in situ cardiac sympathetic nerve endings. *Neurochem Int* 35, 439–445.

Common Sodium Channel Promoter Haplotype in Asian Subjects Underlies Variability in Cardiac Conduction

Connie R. Bezzina, PhD*; Wataru Shimizu, MD, PhD*; Ping Yang, PhD*; Tamara T. Koopmann, BSc; Michael W.T. Tanck, PhD; Yoshihiro Miyamoto, MD, PhD; Shiro Kamakura, MD, PhD; Dan M. Roden, MD; Arthur A.M. Wilde, MD, PhD

Background—Reduced cardiac sodium current slows conduction and renders the heart susceptible to ventricular fibrillation. Loss of function mutations in *SCN5A*, encoding the cardiac sodium channel, are one cause of the Brugada syndrome, associated with slow conduction and a high incidence of ventricular fibrillation, especially in Asians. In this study, we tested the hypothesis that an *SCN5A* promoter polymorphism common in Asians modulates variability in cardiac conduction.

Methods and Results—Resequencing 2.8 kb of *SCN5A* promoter identified a haplotype variant consisting of 6 polymorphisms in near-complete linkage disequilibrium that occurred at an allele frequency of 22% in Asian subjects and was absent in whites and blacks. Reporter activity of this variant haplotype, designated HapB, in cardiomyocytes was reduced 62% compared with wild-type haplotype (P=0.006). The relationship between *SCN5A* promoter haplotype and PR and QRS durations, indexes of conduction velocity, was then analyzed in a cohort of 71 Japanese Brugada syndrome subjects without *SCN5A* mutations and in 102 Japanese control subjects. In both groups, PR and QRS durations were significantly longer in HapB individuals ($P \leq 0.002$) with a gene-dose effect. In addition, up to 28% and 48% of variability in PR and QRS durations, respectively, were attributable to this haplotype. The extent of QRS widening during challenge with sodium channel blockers, known to be arrhythmogenic in Brugada syndrome and other settings, was also genotype dependent (P=0.002).

Conclusions—These data demonstrate that genetically determined variable sodium channel transcription occurs in the human heart and is associated with variable conduction velocity, an important contributor to arrhythmia susceptibility. (*Circulation*. **2006;113:338-344.**)

Key Words: arrhythmia ■ conduction ■ death, sudden ■ genetics ■ ion channels

Sudden cardiac death (SCD) accounts for 20% of all mortality in Western countries.[1] One key determinant of normal excitation and conduction of the cardiac impulse is the cardiac sodium channel, responsible for rapid depolarization in most cardiomyocytes. Reduced sodium current predisposes to SCD. For example, although sodium channel blockers have been used for antiarrhythmic therapy, the Cardiac Arrhythmia Suppression Trial (CAST) showed that these agents increase the incidence of SCD.[2] Loss of function mutations in *SCN5A*, the cardiac sodium channel gene, causes ≈20% of cases of the Brugada syndrome, which is associated with a high risk of SCD.[3] Furthermore, there is evidence that such sodium channel mutations also may lead to enhanced fibrosis in myocardial tissue.[4,5]

Editorial 330
Clinical Perspective p 344

The overall hypothesis underlying the work presented here is that variability in regulation of sodium channel expression contributes to interindividual variability in cardiac conduction and consequently can be considered a candidate modulator of arrhythmia susceptibility, especially in the presence of other stressors such as drugs or acute myocardial ischemia.[6] As a first step in testing this hypothesis, we cloned and characterized the proximal promoter region of *SCN5A* and identified multiple cis-acting elements regulating gene expression.[7] We report here identification of an ethnic-specific, common *SCN5A* promoter variant that modulates PR and QRS durations, indexes of cardiac conduction.

Received August 3, 2005; revision received September 15, 2005; accepted October 11, 2005.

From the Experimental and Molecular Cardiology Group, Department of Experimental Cardiology (C.R.B., T.T.K., A.A.M.W.), Department of Clinical Genetics (C.R.B.), and Department of Clinical Epidemiology and Biostatistics (M.W.T.T.), Academic Medical Center, University of Amsterdam, Amsterdam, the Netherlands; Division of Cardiology, Department of Internal Medicine (W.S., S.K.), and Laboratory of Molecular Genetics (Y.M.), National Cardiovascular Center, Suita, Osaka, Japan; and Department of Medicine and Pharmacology, Division of Clinical Pharmacology, Vanderbilt University School of Medicine, Nashville, Tenn (P.Y., D.M.R.).

*Drs Bezzina, Shimizu, and Yang contributed equally to this study.

Guest Editor for this article was Douglas P. Zipes, MD.

The online-only Data Supplement can be found at http://circ.ahajournals.org/cgi/content/full/CIRCULATIONAHA.105.580811/DC1.

Correspondence to Connie R. Bezzina, PhD, Experimental and Molecular Cardiology Group, Room M0–105, Department of Experimental Cardiology, Academic Medical Center, Meibergdreef 9, 1105 AZ Amsterdam, Netherlands. E-mail C.R.Bezzina@amc.uva.nl

Circulation **is available at http://www.circulationaha.org** **DOI: 10.1161/CIRCULATIONAHA.105.580811**

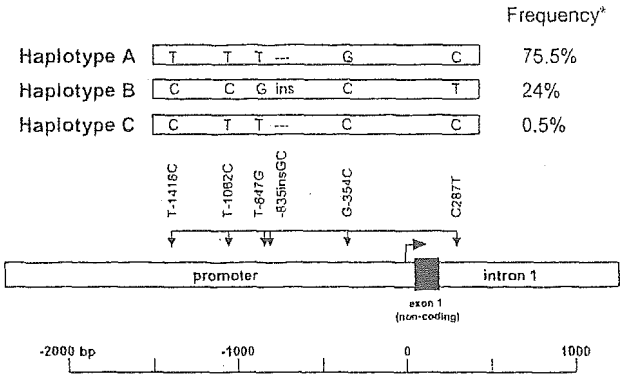

Figure 1. Haplotypes identified in the cardiac sodium channel gene (*SCN5A*) promoter. Nucleotide variations are indicated by their position relative to the major transcription initiation site (+1),[7] with the most frequent nucleotide given below and the least frequent nucleotide given above the position. *Frequency in the Japanese (control) population.

Methods

Identification of Polymorphisms

Resequencing 2.8 kb of the *SCN5A* promoter region in a single individual of Asian origin identified him as a homozygote for 6 DNA polymorphisms in the region: T-1418C, T-1062C, T-847G, −835insGC, G-354C, and C287T (Figure 1). The resequenced region encompassed positions −2190 to 613, relative to the major transcription initiation site[7] of the *SCN5A* promoter, including 2.2 kb upstream of exon 1, exon 1 (which is 173 bp and noncoding), and the proximal 439 bp of intron 1. The fragment was amplified by long and accurate polymerase chain reaction (PCR; TaKaRa kit) with primers F1 and R1 (Data Supplement Table I; see http://circ.ahajournals.org/cgi/content/full/CIRCULATIONAHA.105.580811/DC1). Further studies described below established that these polymorphisms were common and in near-total linkage disequilibrium, thereby identifying 2 common haplotype blocks, designated HapA and HapB. We also detected a third combination of polymorphisms, designated HapC, in <1% of subjects. In addition to the study populations, 150 white and 100 black individuals were tested for these haplotypes.

Functional Analysis

Generation of Constructs

The 2.8-kb fragment described above was amplified from genomic DNA of HapA- and HapB-homozygous individuals. These fragments were cloned into the pGEM-T Easy vector (Promega), and inserts were subsequently subcloned into the pGL3-basic vector (Promega), which contains the firefly luciferase coding sequence, to generate *SCN5A* promoter–luciferase fusion constructs for reporter assays. These constructs were designated pGL3-Hap A and pGL3-Hap B.

Reporter Activity

Reporter activity was assayed in neonatal mouse cardiomyocytes and in Chinese hamster ovary cells as described in detail previously.[7] In brief, 1 μg pGL3-Hap A or pGL3-Hap B was transfected into neonatal mouse cardiomyocytes or Chinese hamster ovary cells. In each experiment, 0.05 μg pRL-TK plasmid (Promega) encoding Renilla luciferase was cotransfected to normalize for experimental variability caused by differences in cell viability or transfection efficiency. Luminescence was measured 48 hours after transfection with the Dual-Luciferase Reporter Assay System (Promega). The pGL3-basic (promoterless) plasmid was tested in each experiment; its activity level served as the baseline.

Study Participants

Participants in the clinical study were ascertained at the National Cardiovascular Center (Osaka, Japan). All protocols (including molecular screening) were reviewed and approved by the Ethical Review Committee of the National Cardiovascular Center, and informed consent was obtained from all individuals.

The control population consisted of 102 subjects drawn from mutation-negative relatives in congenital long-QT syndrome families in which the causative mutation had been identified. Only 1 person was drawn from each family. There were 67 male and 35 female subjects ranging from 9 to 69 years of age; mean age was 40±14 years (mean±SD).

The Brugada syndrome population included 80 patients diagnosed with Brugada syndrome, defined as type 1 "coved" ST-segment elevation in V_1 through V_3 (spontaneous in 70 patients, induced by sodium channel blocker in 10 patients).[8] In all patients, physical examination, chest roentgenogram, laboratory values, echocardiography with wall motion analysis, and Doppler screening excluded structural heart disease. Aborted cardiac arrest or ventricular fibrillation (VF) was documented in 30 patients, syncope was identified in 20, and 30 were asymptomatic. All patients had previously been screened for *SCN5A* coding region mutations, and a mutation had been identified in 9 patients. The patient group included 76 male and 4 female subjects ranging from 1 to 76 years of age (mean±SD, 47±16 years).

ECG Phenotypes

ECGs were assessed by an investigator (W.S.) who was blinded to age, gender, and genetic and clinical information. Phenotypes assessed included RR interval, PR interval measured in lead II (PR_{II}), QRS interval measured in leads V_1 (QRS_{V1}) and V_6 (QRS_{V6}), ST amplitude at J point (ST_J), and ST amplitude at 80 ms after the end of the QRS (ST_{80}).

The effects of intravenous administration of sodium channel blockers on these ECG parameters were examined in 49 of 80 Brugada syndrome patients. Pilsicainide (maximum 1 mg/kg at a rate of 0.1 mg · kg^{-1} · min^{-1}) was used in 37 patients, flecainide (maximum 2 mg/kg at a rate of 0.2 mg · kg^{-1} · min^{-1}) was used in 9 patients, and disopyramide (maximum 2 mg/kg at a rate of 0.2 mg · kg^{-1} · min^{-1}) was used in 3 patients.

Genotyping

Genomic DNA was prepared from blood leukocytes. Genotyping for the T-1418C and T-1062C single nucleotide polymorphisms (SNPs) was performed by restriction fragment length polymorphism analysis after PCR amplification with *Ear*I and *Hae*III, respectively. PCR primers used to amplify the 161-bp fragment encompassing the T-1418C SNP were F2 and R2, and those used to amplify the 123-bp fragment encompassing the T-1062C SNP were F3 and R3 (Data Supplement Table II). Genotyping for the other 4 polymorphisms (T-847G, 835insGC, G-354C, and C287T) was done by DNA resequencing of both strands. PCR primers used to amplify the 638-bp fragment encompassing the T-847G, 835insGC, and G-354C polymorphisms were F4 and R4; those used to amplify the 599-bp fragment encompassing the C287T polymorphism were F5 and R5.

Statistical Analysis

Using the individual genotypes for the 6 polymorphisms, we estimated haplotype frequencies using an E-M algorithm.[9] The haplotype frequencies were used to calculate the probabilities of the haplotype pairs compatible with the genotype combinations of the multiple heterozygous patients using Bayes' theorem. Observed haplotype pair frequencies were compared with those expected under Hardy-Weinberg equilibrium in the Brugada syndrome population and control population separately with a χ^2 test. To compare haplotype pair frequencies among Brugada syndrome patients and control subjects, Fisher's exact test was used.

All quantitative phenotypes were normally distributed, and data are expressed as mean±SD. Continuous ECG phenotypes were compared between *SCN5A* mutation–negative Brugada syndrome patients, *SCN5A* mutation–positive Brugada syndrome patients, and control subjects by ANOVA adjusted for age and gender, followed by a post hoc test for pairwise comparisons. Student *t* tests were used

to compare the after-drug-challenge continuous ECG phenotypes between *SCN5A* mutation–negative and –positive Brugada syndrome patients. Correlations between quantitative phenotypes before and after sodium channel blockade are expressed as Pearson correlation coefficients (r). For comparison of the proportion of male subjects, Fisher's exact test was used.

The effect of haplotype pairs on the continuous ECG phenotypes was tested in the Brugada syndrome patients and control subjects separately by ANOVA with adjustment for age and gender. The 9 *SCN5A* mutation–positive Brugada syndrome patients were treated as a separate category (7 HapA/HapA homozygotes, 2 HapA/HapB heterozygotes, pooled). The 2 individuals with the rare HapC variant (1 patient from each group) were excluded from analyses. In all analyses, the proportion of variance attributable to the haplotype pair (R^2) was calculated and corrected for the effects of age and gender.

Differences in reporter gene expression activity between HapA and HapB were examined for statistical significance with Student's t test. Throughout, values of $P<0.05$ were interpreted as being significant. All statistical analyses were done with SAS software (version 9, SAS Institute).

Multiple Testing

When a Bonferroni correction for the 24 statistical models is used to compare the continuous ECG phenotypes, the significance level for the overall probability values is 0.002. Similarly, the Bonferroni-corrected significance levels for the pairwise comparisons between 3 and 4 groups is 0.017 and 0.008, respectively.

Results

Haplotypes

The 6 polymorphisms were in near-complete linkage disequilibrium, with only 2 (similar) discordant haplotypes (of 364; <1%), each occurring in 1 subject from each population. We designated HapA as containing all common alleles and HapB as containing all minor alleles (Figure 1). The discordant haplotype was designated HapC. The estimated frequencies of HapA, HapB, and HapC were 0.755, 0.240, and 0.005 in the control subjects and 0.782, 0.211, and 0.007 in the *SCN5A* mutation–negative Brugada syndrome patients, respectively. Haplotype distributions were in Hardy-Weinberg equilibrium ($P>0.05$) in both populations. No significant difference in haplotype frequencies was observed between the Brugada syndrome group and the control subjects. The haplotypes were absent in white and black samples.

Functional Analysis

In cardiomyocytes, reporter activity of HapB was markedly reduced, by 62%, compared with HapA: 5.5±0.4 (mean±SE) versus 14.5±2.8 (normalized activity units; n=9 each; $P=0.006$; Figure 2). A similar trend was seen in the noncardiac cells: 2.7±0.3 versus 3.6±0.3 (n=13 each; $P=0.04$; Figure 2).

Phenotypic Characteristics of the Control and Brugada Syndrome Patient Populations

The decreased reporter activity for HapB suggested that individuals carrying this promoter haplotype would display ECG-detectable conduction slowing. Accordingly, the relationships between genotype and ECG intervals were evaluated in the control and Brugada syndrome populations.

ECG data are shown in Table 1. As expected, Brugada syndrome patients had significantly longer conduction intervals (PR_{II}, QRS_{V1}, QRS_{V6}) and greater ST-segment elevation

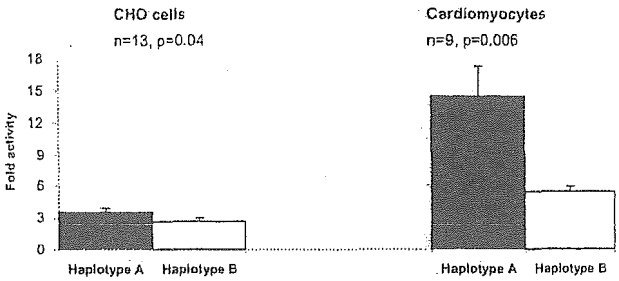

Figure 2. Reporter activity of *SCN5A* promoter haplotypes A and B. Firefly luciferase expression levels, which report the activities of the inserted *SCN5A* sequence, were divided by coexpressed Renilla luciferase activities and expressed as relative luciferase units.[7] Data are presented as mean±SE (vs empty vector). CHO indicates Chinese hamster ovary.

(ST_J, ST_{80}) compared with control subjects. Heart rate was not significantly different between the 2 populations. In addition, we found differences between *SCN5A* mutation–positive and *SCN5A* mutation–negative Brugada syndrome patients similar to those previously reported[10]: Mutation-positive subjects had significantly longer baseline PR and QRS intervals and longer RR intervals. Data on the subset of Brugada syndrome patients who underwent drug challenge are presented in Table 2. For all ECG parameters investigated, highly significant ($P<0.0001$) correlations were present between measures before and after drug challenge (Table 2). As previously reported, *SCN5A* mutation–positive patients displayed longer PR and QRS intervals after challenge with sodium channel blockers compared with *SCN5A* mutation–negative patients.[10]

Haplotype Pair Effects

PR and QRS durations were significantly longer in HapB individuals in both study populations (Brugada syndrome and control subjects: $P\leq0.002$ for PR_{II}; $P<0.0001$ for QRS_{V1} and QRS_{V6}; Figure 3). In the control population, PR_{II}, QRS_{V1}, and QRS_{V6} intervals showed a gene-dose effect, being longest in HapB homozygotes, intermediate in HapA/HapB heterozygotes, and shortest in HapA homozygotes. A similar pattern was observed in the *SCN5A* mutation–negative Brugada syndrome patient group. As discussed earlier, these analyses excluded data in the 2 individuals with HapC. PR_{II}, QRS_{V1}, and QRS_{V6} means (±SD) per haplotype group for the 2 populations are listed in the Data Supplement Table II. Both the overall and pairwise probability values were highly statistically significant even after correction for multiple testing.

The amount of variance (R^2) in PR and QRS intervals explained by the haplotype pair after correction for age and gender is shown in Table 3. As can be seen, a significant proportion of variance in PR and QRS intervals, both at baseline (both groups) and after drug challenge (Brugada syndrome group), was attributable to the haplotype. No significant association was found between haplotype and RR, ST_J, and ST_{80} in either population (data not shown).

Drug Challenge and Haplotype

The haplotype pairs were also highly associated with conduction intervals (PR_{II}, QRS_{V1}, QRS_{V6}) after sodium channel

TABLE 1. Baseline ECG Characteristics of the Control and Brugada Syndrome Patient Populations

		Brugada Syndrome Patients			Pairwise Comparison *P*	
	Control Subjects	*SCN5A*$^{-ve}$	*SCN5A*$^{+ve}$	Overall *P*	*SCN5A*$^{-ve}$ vs *SCN5A*$^{+ve}$	*SCN5A*$^{-ve}$ vs Control Subjects
n	102	71	9			
Male, n (%)	67 (66)	67 (94)	9 (100)	<0.0001	1.000	<0.0001
Age, y	40.0±14.2	46.5±16.3	51.1±8.4	0.005	0.376	0.005
RR, ms	925.3±130.0	913.7±134.3	1055.6±154.2	0.012	0.003*	0.572
PR_{II}, ms	162.3±21.8	180.4±20.4	238.9±26.7	<0.0001*	<0.0001*	<0.0001*
QRS_{V1}, ms	93.8±11.8	104.9±19.3	142.2±19.1	<0.0001*	<0.0001*	<0.0001*
QRS_{V6}, ms	87.4±12.4	100.2±19.1	139.4±21.6	<0.0001*	<0.0001*	<0.0001*
ST_J, mV	0.10±0.05	0.30±0.14	0.34±0.18	<0.0001*	0.249	<0.0001*
ST_{80}, mV	0.18±0.10	0.25±0.12	0.24±0.13	0.001*	0.778	0.001*

Values are given as mean±SD.
*Below the Bonferroni-corrected overall or pairwise significance levels (see Multiple Testing).

blockade in 44 *SCN5A* mutation–negative Brugada syndrome patients who underwent drug challenge (for PR_{II}, QRS_{V1}, QRS_{V6}, $P<0.0001$; Figure 3). PR_{II}, QRS_{V1}, and QRS_{V6} means (±SD) per haplotype group are listed in the Data Supplement Table II. Here also, overall and pairwise probability values were highly statistically significant even after correction for multiple testing.

In addition, the extent of QRS widening (ΔQRS) after drug challenge was genotype dependent, and a gene-dose effect was also observed (ΔQRS_{V6}: HapB/HapB=30 ms [mean± SD]; HapA/HapB=24.2±7.9; HapA/HapA=17.8±7.2; $P=0.002$; Figure 4). A similar trend was seen for extent of PR widening (ΔPR) after drug challenge (ΔPR_{II}: HapB/HapB=40 ms; HapA/HapB=33.8±13.2; HapA/HapA=28.6±8.3; $P=0.05$).

Discussion

We demonstrate that a set of 6 *SCN5A* promoter polymorphisms found in Asian subjects are in near-complete linkage disequilibrium, have a significant impact on sodium channel expression in vitro, account for a large proportion of variance in ECG conduction parameters in 2 independent Japanese populations, and represent pharmacogenetic markers predicting variable drug response.

Twin studies have identified strong genetic effects for ECG parameters, including PR and QRS durations.[11–14] Indeed, associations have been reported between ECG parameters and single coding region nonsynonymous (amino acid–changing) SNPs in ion channel genes.[15,16] However, common functional variants in regulatory regions that strongly modulate basal ECG intervals have not previously been identified; 1 preliminary report has suggested an association between a potassium channel promoter polymorphism and QRS axis in women only.[17] Only recently has the concept of tightly linked polymorphisms (constituting a haplotype block) been applied to understanding variability in cardiac electrophysiology. In 1 study, a small degree of variance (<1%) in QT interval in a central European population could be attributed to single SNPs and haplotype blocks in 4 potassium channel genes.[18]

TABLE 2. Clinical Characteristics of the Brugada Syndrome Patients After Sodium Channel Blocker Challenge

	SCN5A^{-ve}	*SCN5A*$^{+ve}$	*P*	*r*, Before and After Sodium Channel Blockade
n	44	5		
Male, n (%)	42 (95)	5 (100)	1.000	
Age, y	46.3±14.8	52.0±5.4	0.397	
aRR, ms	892.3±113.1	956.0±99.4	0.234	0.94
aPR_{II}, ms	209.6±25.1	278.0±35.6	<0.0001*	0.95
$aQRS_{V1}$, ms	124.1±16.1	166.0±17.8	<0.0001*	0.92
$aQRS_{V6}$, ms	119.2±17.1	166.0±17.8	<0.0001*	0.92
aST_J, mV	0.51±0.21	0.78±0.25	0.013	0.84
aST_{80}, mV	0.41±0.17	0.70±0.31	0.109	0.63

Values are given as mean±SD. Pearson correlation coefficients (*r*) observed between measures before and after sodium channel blocker challenge ($P<0.0001$). Mean baseline ECG parameters for the 44 *SCN5A*$^{-ve}$ and 5 *SCN5A*$^{+ve}$ patients (not shown) were very similar to those for the total patient group given in Table 1.
*Below the Bonferroni-corrected overall significance levels (see Multiple Testing).

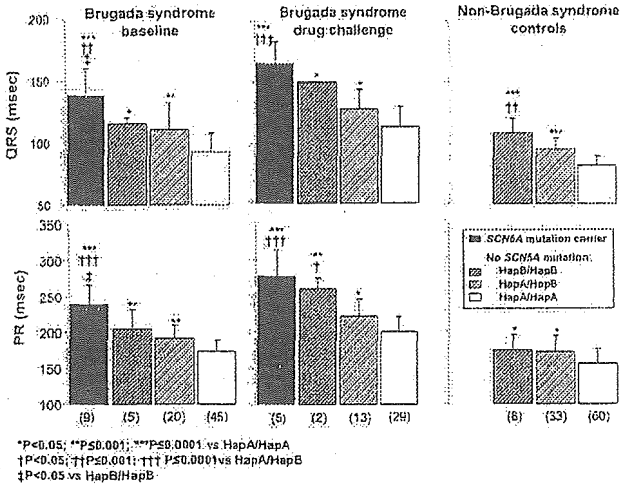

Figure 3. *SCN5A* promoter haplotype effects on durations of QRS_{V6} and PR_{II} in Brugada syndrome patients at baseline and after challenge with sodium channel blocking agents and in non–Brugada syndrome control subjects. Patient numbers are indicated in parentheses. Genotype effects on QRS_{V1} were similar to those on QRS_{V6} because of a high correlation between these 2 parameters (Pearson's coefficient, r=0.96). Data are presented as mean±SD. For Bonferroni-corrected significance levels for pairwise comparisons, refer to the Multiple Testing section in Patients and Methods.

In contrast, the *SCN5A* promoter haplotype we report here explained a remarkable proportion of variance in conduction parameters in the Japanese subjects studied (Table 3). Such associations could arise because the haplotypes studied are, in turn, in linkage disequilibrium with other functionally important variants in regulatory or other regions of the gene. However, in this case, the in vitro functional studies indicate that the effect is attributable to a variant within the haplotype block; at this point, the specific variant mediating this effect has not been identified.

A principal determinant of cardiac conduction in atrial and ventricular muscle is the sodium current; sodium channel blockers prolong PR and QRS durations, an effect also seen with loss of function mutations in *SCN5A*.[3] Critical degrees of conduction slowing represent a final common pathway to VF,[19] so dissection of the genetic determinants of cardiac conduction in the general population is a key step to understanding variable susceptibility to common arrhythmias resulting from conduction slowing, as in myocardial ischemia

TABLE 3. Variance Explained by the Haplotype Pair

	R^2, %		
	Control Subjects	Brugada Syndrome Baseline	Brugada Syndrome Drug Challenge
PR_{II}	12.2	28.4	33.0
QRS_{V1}	47.6	26.4	33.0
QRS_{V6}	48.5	24.9	36.2

or heart failure.[19] Thus, the data we present here implicate the *SCN5A* promoter variant HapB, which slowed conduction in normal subjects and exacerbated conduction slowing in those with Brugada syndrome, as a candidate modulator of variability in risk of SCD. Importantly, imposition of further depression of sodium channel function by administration of sodium channel blocking drugs further exacerbated conduction slowing in a gene-dose-dependent fashion. Studies in large numbers of subjects at risk for SCD are required to further establish the role of this and other regulatory region polymorphisms in modulating that risk.

Differences in disease penetrance and expression have been widely reported in the cardiac sodium and other channelopathies.[20–23] Relatives carrying an *SCN5A* mutation identical to that of the proband may be clinically unaffected,[20] and family members may display different phenotypes, eg, Brugada syndrome or conduction disease.[23] Genetic variants like the one presented here are obvious candidate modulators of this variability in phenotypic expression. Interindividual variability also has been noted in response to pharmacological challenge with sodium channel blockers in Brugada syndrome patients.[20,24] In some patients, even some carrying an *SCN5A* mutation, drug challenge fails to unmask a Brugada syndrome ECG. The significantly greater increases in PR and QRS durations with sodium channel blockade in HapB carriers thus identify variability in expression of the drug target, the sodium channel, as a key mediator of this variable drug effect. It is thus possible that other sodium channel blocker response phenotypes such as the increased mortality with sodium channel blockers in the CAST[2] was determined by variable sodium channel expression. DNA samples from that important clinical trial were not archived, so this question will remain unanswered. More generally, the data

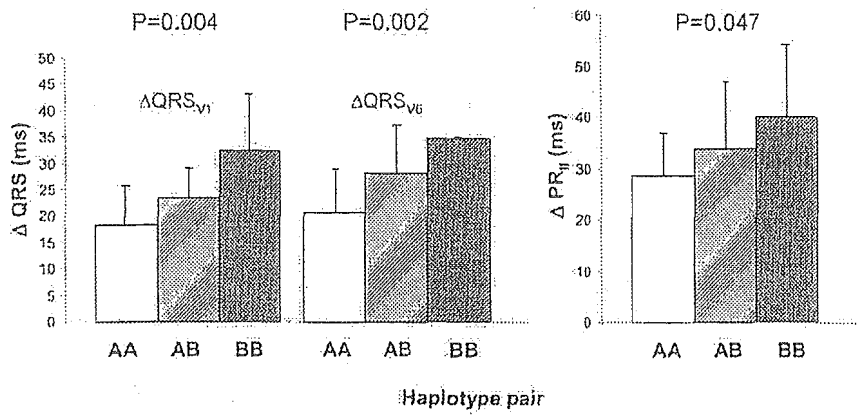

Figure 4. *SCN5A* promoter haplotype effects on extent of QRS (ΔQRS_{V1} and ΔQRS_{V6}) and PR (ΔPR_{II}) widening after sodium channel blockade. AA, n=29; AB, n=13; BB, n=2. Data are presented as mean±SD. The Bonferroni-corrected significance level is 0.002.